AFRL-PR-WP-TR-2004-2060

PROPULSION AND POWER RAPID RESPONSE R&D SUPPORT
Delivery Order 0013: Micro Gas Chromatography Tradeoff Study

By:

Ulrich Bonne (Honeywell Labs)
Gary Eden (University of Illinois)
Greg Frye-Mason (Nomadics, Inc.)
Richard Sacks (University of Michigan)
Rob Synovec (University of Washington)

Honeywell Labs
12001 State Hwy 55
Plymouth, MN 55441

For:

Universal Technology Corporation
1270 North Fairfield Road
Dayton, OH 45432-2600

NOVEMBER 2003

Final Report for 28 June 2003 – 19 November 2003

Approved for public release; distribution is unlimited.

STINFO FINAL REPORT

PROPULSION DIRECTORATE
AIR FORCE MATERIEL COMMAND
AIR FORCE RESEARCH LABORATORY
WRIGHT-PATTERSON AIR FORCE BASE, OH 45433-7251

NOTICE

USING GOVERNMENT DRAWINGS, SPECIFICATIONS, OR OTHER DATA INCLUDED IN THIS DOCUMENT FOR ANY PURPOSE OTHER THAN GOVERNMENT PROCUREMENT DOES NOT IN ANY WAY OBLIGATE THE U.S. GOVERNMENT. THE FACT THAT THE GOVERNMENT FORMULATED OR SUPPLIED THE DRAWINGS, SPECIFICATIONS, OR OTHER DATA DOES NOT LICENSE THE HOLDER OR ANY OTHER PERSON OR CORPORATION; OR CONVEY ANY RIGHTS OR PERMISSION TO MANUFACTURE, USE, OR SELL ANY PATENTED INVENTION THAT MAY RELATE TO THEM.

THIS REPORT IS RELEASABLE TO THE NATIONAL TECHNICAL INFORMATION SERVICE (NTIS). AT NTIS, IT WILL BE AVAILABLE TO THE GENERAL PUBLIC, INCLUDING FOREIGN NATIONS.

THIS TECHNICAL REPORT HAS BEEN REVIEWED AND IS APPROVED FOR PUBLICATION.

/s/
THOMAS L. REITZ, Ph.D.
Project Engineer
Energy Storage & Thermal Sciences Branch

/s/
JOHN G. NAIRUS
Chief
Energy Storage & Thermal Sciences Branch

/s/
CYNTHIA A. OBRINGER
Deputy Chief
Power Division
Propulsion Directorate

Do not return copies of this report unless contractual obligations or notice on a specific document require its return.

REPORT DOCUMENTATION PAGE

Form Approved
OMB No. 0704-0188

The public reporting burden for this collection of information is estimated to average 1 hour per response, including the time for reviewing instructions, searching existing data sources, searching existing data sources, gathering and maintaining the data needed, and completing and reviewing the collection of information. Send comments regarding this burden estimate or any other aspect of this collection of information, including suggestions for reducing this burden, to Department of Defense, Washington Headquarters Services, Directorate for Information Operations and Reports (0704-0188), 1215 Jefferson Davis Highway, Suite 1204, Arlington, VA 22202-4302. Respondents should be aware that notwithstanding any other provision of law, no person shall be subject to any penalty for failing to comply with a collection of information if it does not display a currently valid OMB control number. **PLEASE DO NOT RETURN YOUR FORM TO THE ABOVE ADDRESS**.

1. REPORT DATE *(DD-MM-YY)*	2. REPORT TYPE	3. DATES COVERED *(From - To)*
November 2003	Final	06/28/2003 – 11/19/2003

4. TITLE AND SUBTITLE
PROPULSION AND POWER RAPID RESPONSE R&D SUPPORT
Delivery Order 0013: Micro Gas Chromatography Tradeoff Study

5a. CONTRACT NUMBER
F33615-02-D-2299-0013

5b. GRANT NUMBER

5c. PROGRAM ELEMENT NUMBER
62203F

6. AUTHOR(S)
Ulrich Bonne (Honeywell Labs)
Gary Eden (University of Illinois)
Greg Frye-Mason (Nomadics, Inc.)
Richard Sacks (University of Michigan)
Rob Synovec (University of Washington)

5d. PROJECT NUMBER
3145

5e. TASK NUMBER
13

5f. WORK UNIT NUMBER
0H

7. PERFORMING ORGANIZATION NAME(S) AND ADDRESS(ES)

By:	For:
Honeywell Labs 12001 State Hwy 55 Plymouth, MN 55441	Universal Technology Corporation 1270 North Fairfield Road Dayton, OH 45432-2600
University of Illinois Nomadics, Inc. University of Michigan University of Washington	

8. PERFORMING ORGANIZATION REPORT NUMBER

9. SPONSORING/MONITORING AGENCY NAME(S) AND ADDRESS(ES)
Propulsion Directorate
Air Force Research Laboratory
Air Force Materiel Command
Wright-Patterson AFB, OH 45433-7251

10. SPONSORING/MONITORING AGENCY ACRONYM(S)
AFRL/PRPS

11. SPONSORING/MONITORING AGENCY REPORT NUMBER(S)
AFRL-PR-WP-TR-2004-2060

12. DISTRIBUTION/AVAILABILITY STATEMENT
Approved for public release; distribution is unlimited.

13. SUPPLEMENTARY NOTES
Report contains color.

14. ABSTRACT

This effort seeks to extend the effort of the Dec.'02 DARPA Workshop on Micro Gas Analyzers (MGAs) to focus on the application of a Micro Gas Chromatograph (MGC). The primary goal of this study is to project MGA capabilities in terms of goals for compactness, sensitivity, selectivity, false positives avoidance, analysis time, and energy-per-analysis (≤ 2 cm^3, ≤ 10 ppt, ≥ 15 target compounds, false positive rate $\leq 1/288{,}000$, ≤ 3 s, and ≤ 1 J/analysis). Secondary objectives include identification, exploration, and quantification of associated tradeoffs among such capabilities and facilitation of such quantification with the inclusion of easy-to-use mathematical modeling tools running on Excel. Technical hurdles which might accompany MGA development are discussed, and a methodology to overcome them is presented.

15. SUBJECT TERMS

16. SECURITY CLASSIFICATION OF:			17. LIMITATION OF ABSTRACT:	18. NUMBER OF PAGES	19a. NAME OF RESPONSIBLE PERSON (Monitor) / 19b. TELEPHONE NUMBER *(Include Area Code)*
a. REPORT	b. ABSTRACT	c. THIS PAGE			
Unclassified	Unclassified	Unclassified	SAR	58	Thomas L. Reitz (937) 255-4275

Standard Form 298 (Rev. 8-98)
Prescribed by ANSI Std. Z39-18

Table of Contents **Page**

MICRO GAS CHROMATOGRAPHY TRADEOFF STUDY
Final Report

SUMMARY AND SCOPE

In extending the effort of the Dec.'02 DARPA Workshop on Micro Gas Analyzers (MGAs)[1], the purpose of this study was to focus on one type of MGA, the Micro Gas Chromatograph (MGC), to:

- Project its ultimate capabilities in terms of goals for compactness, sensitivity, selectivity, false-positives-avoidance, analysis time and energy-per-analysis, ($\leq$ 2 cm^3, $\leq$ 10 ppt, $\geq$ 15 target compounds, false positive rate $\leq$ 1/288,000, $\leq$ 3 s, and $\leq$ 1 J/analysis)
- Identify, explore and quantify associated tradeoffs among such capabilities and to facilitate such quantification with the inclusion of easy-to-use mathematical modeling tools running on Excel
- Define and keep track of technical hurdles that may need to be overcome.

Deliverable and related MGC mathematical performance models and bench-marking relative to competing technologies were logical additions to the above. Our team was tasked to complete this 3-month study at a kick-off meeting at DARPA on 16 July 2003 and provided details on how to meet the objectives.

This final report thus supersedes the earlier, interim version[8] and includes additional "In-Depth Reports" and chapters, see below, on detector technology, GC separation technology, and on detector statistics.

GC technology, its development needs and hurdles to be overcome: Insights on this subject, gained during this Study and the period of time leading up to it and which impact the purpose stated above, may be summarized as follows:

Micro Gas Analyzer Technology Insights- General:

- **Optimal Performance:** Optimal and simultaneous selectivity and sensitivity performance on multiple known and future target analytes is best achieved with analyzers that synergize the analyte separation and detection function, especially in terms of minimizing the probability of false positives
- **Maximally Competitive MGAs** would be those in which the **selectivity and detection functions are optimized and performed separately**, rather than integrating them into one operational step, as for example in a system comprising an array of chemi-resistors, or a fixed laser as light source for opto-acoustic detection.
- **The Probability of False Positives**, P_{fp}, drops as we increase the number of individual, independent and/or orthogonal measurements on an unknown gas mixture, which contains the target analytes and a number of interfering gases. An important requirement is to have a signal that is clearly above the noise and drift level.
- **The total number measurements** contributing towards P_{fp} reduction, may be defined as the product of the number of independent measurements provided by each of the m different measurement methods, $n = n_1 \times n_2 \times ....n_m$. For the example of a μGC-μMS analyzer, n = 50x100 = 5000, rather than 50+100, assuming that we can achieve a μGC peak capacity of n_1 = 50 and a MS mass peak capacity of n_2 = 100.
- **MGA networking** and its associated logic can provide an additional factor of ~100x reduction in the rate of false positives
- **Uniqueness of MGCs**: MGCs as "boiling point spectrometers" stand out among MGAs because they not only separate components of a mixture but also provide enough individual material quantities for further analysis, which facilitates reduction in P_{fp}.

Micro GC Technology Insights:

- **Thin MGC Films** for both the stationary phase and its support are key to simultaneously achieve high-speed pre-concentration, separation and maximum resolution/peak capacity, while minimizing power consumption. For example thermal time constants of 0.8 ms were predicted for heated films of ~2 μm in thickness, and confirmed experimentally, as was the power requirement of 2.2 mJ for a 5 ms heater pulse to raise its temperature by 180°C.

- **Micro-GC Peak Capacities** of about 50 may be achievable with suitable temperature programming of the separation column and further R&D on stationary phase film materials to approach theoretical performance of H/d =1, where H = theoretical plate height and d = diameter of the capillary
- **Resolution and Temperature Ramping.** Temperature ramping of the separation column increases the peak capacity, which is also related to GC resolution and in turn to the isothermal capacity factor, $k'=(t_R-t_o)/t_o$. "R.Sack's rule" provides guidance on the effect of temperature: k' is halved for every 17°C rise, so that by ramping at an optimal TBD rate, e.g. near ~17°C for every doubling in the retention time, t_R, the peak width (which really depends on H(T)) can be maintained throughout the scheduled elution time, and thus maximize peak capacity. Another guideline is to ramp the temperature at such a rate that the eluting compound boiling point stays in about a constant ratio to the column temperature.
- **Compactness Limit**: As we strive for ultimate MGC compactness, one formidable constraint on achievable resolution with ever smaller μGCs is pressure drop, as it limits the length of a capillary column and thus the achievable resolution

Micro GC Tradeoffs, Development Needs and Technical Hurdles:

- **Predicting Pfp**: Translate the need for meeting a maximum rate or probability of false positives into statistical/deterministic terms such as signal/noise ratio and number of independent measurements. The essay in Section 5 provides details on one approach to this challenge
- **Low Limit to Column Size:** Research the performance of μGCs operating with columns at and below 100 μm diameter, with sub-micron films to achieve the needed speed, yet of short enough length to stay within a practical pressure drop (about ≤ 10 psi), with due consideration for the effects of finite sample plug width
- **Sample Gas Transport**: GC operation critically depends on reliable sample (or carrier) gas flow control, which is now dependent on failure-prone mechanical devices. Therefore alternatives to mechanical gas pumping and flow control should be explored. There is an unmet need for smoother, more compact, more reliable and low-power gas pumps and flow control valves.
  The essay in Section 7 provides details on some approaches to this challenge
- **Interim Sample Gas Transport:** Select or develop compact and low-power mechanical μvalves and μpumps for reliable control of sub cm^3/minute sample gas flow rate as an interim solution
- **Largest MGC Energy Consumer**: Temperature ramping of a MGC column is the part that consumes the largest part of energy per analysis, and means to reduce it without affecting the structural integrity of the MGC are needed.
- **Advanced Selectivity:** Search and identify materials combinations for pre-concentration, GC-GC-separation and detection in wet or dry air as carrier gas that support analysis of the target compounds, be they fuel vapor or combustion exhaust constituents, cabin air quality contaminants or CWAs
- **Interference by Water Vapor:** As the target analytes are pre-concentrated, the high (up to 40,000 ppm) concentration, polarity and easy condensation of water vapor from sample air might swamp the concentrator and separator column films. One would therefore try to design at least the first-level pre-concentrator film that is hydrophobic and just passes the water vapor w/o adsorption, as has been observed to be the case with graphitic carbon film columns and other hydrophobic materials.
- **High-Speed Detectors:** Research and develop μGC-compatible detector alternatives that meet millisecond response time and nanoliter dead volume requirements. Examples: Thin polymer films generating variable-stress on micro cantilevers, thin-film resonators (SAW detectors, cantilevers or QCMs); and micro-miniaturized traditional GC detectors
- **Short Injection Times:** To achieve the desired resolution within the allotted ~1 second GC separation time, technologies to achieve short analyte injection pulses are needed. Short "electronic" injection via thermal pulses to the last thin-film segment of a PHASED pre-concentrator[7] and smart mechanical injection schemes (see R.Synovec's Report in the Appendix) are some of the ongoing research efforts.
- **System Simulation and Modeling**: Incorporate the capability to predict column material temperature effects (column temperature programming and its influence on peak capacity) into GC performance models

- **Manufacturability Considerations:** Beyond R&D successes, ultimate success in the eyes of potential users requires that researched MGA designs and capabilities can translate into manufacturable and economically viable products. It is therefore prudent to keep also this cost-benefit tradeoff aspect of MGA research in mind.

Scope; Within the above-stated purpose, we are focusing this seedling effort on these key aspects of μGC functions :

- Pre-concentration
- Separation
- Sample gas transport and flow control
- Detection and molecule identification
- Competitive advantage
- Estimation of False Positives
- MGC Performance Simulation and Modeling
- DoD-relevant applications
- Technology hurdles

A. INTRODUCTION, BACKGROUND AND GOALS

We present here the preliminary results of our review of the MGC-based identification and trace gas detection limit of gaseous analytes, whether encountered as air pollutants, chemical agents or other diagnostic indicators (fuels, medical, machinery, industrial processes) with emphasis on the pros and cons of direct or **simple detection** vs. detection after pre-processing via some pre-concentration and/or analytical separation, better referred to as **composite detection** or multi-dimensional analysis. We discuss the strongest features of both approaches before drawing conclusions about their relative merits for DoD and non-DoD applications.

The overriding figure of merit for the considered approaches has emerged as the probability of "false positive" errors, i.e. the probability of signaling the presence and concentration of certain gases such as CWAs, when they are not present, in an environment in which significant concentrations from fuel oil, equipment fires and explosives handling and combustion might interfere. We have analyzed and derived a model for the makeup of the **"false positive"** probability in terms of its relation to known and measurable "sensor" attributes such as repeatability, S/N, number of independent measurands, cross-sensitivity and multi-dimensional analysis. With the original figures of merit discussed at the last DARPA Workshop on Micro Gas Analyzers in December 2002(1) and their subsequent evolution, the complete and growing list is now:

- Analysis time ≤ 4 seconds for at least 15 compounds,
- Size ≤ 2 cm^3,
- Analysis sensitivity of ≤ 0.001-10 ppb (equivalent to 4-40,000 ng/m^3 of analytes of m.w. = 96 g/mol)
- Analysis energy ≤ 1 J or an average of ≤ 250 mW during the above analysis time period
- Specificity expressed as probability of false positives ≤ 1:180,000, which recently expanded to ≤ 1/288,000(2), and a low false negative rate (exact value not specified).

We will refer to these as the "DARPA Goals" in the pages below. Regarding the choice of organizing a Report written by several contributors, we have traded off a comprehensive integration and "filtration" effort, in favor of enclosing intact all the reports from this Study's Team Members, despite the resulting increased length of the report.

B. DISCUSSION

1. Micromiaturization as Enabler. Microminiaturization of gas analyzers, and especially of MGC, may be viewed as enablers to achieve the above design/performance goals. Especially multi-stage, micro

pre-concentration (PC) was identified as a winning proposition for its >10,000x reduction in the operational energy and power needs, relative to conventional PCs. A summary list compiled to date of the benefits of MGCs in terms of approaching to meet DARPA Goals, relative to conventional analyzers is as follows, for a premium of only a possible 1.2-4x reduction in peak capacity:

- **Decreased MGC system linear size by >20x** (30 cm --> 1.5 cm)
- **Decreased weight by >400** (50 lbs --> 50 g)
- **Decreased analysis time by 100x** (300 s --> 3 s)
- **Decreased power and energy consumption by >1000-10,000x**
- **Increased sensitivity range by >1000x,** via multi-stage pre-concentration by over a factor of 1000, whereby such pre-concentration can be added for little additional cost to a micro GC, and by incorporation of highly sensitive detectors.
- **Expanded number of identifiable analytes in a mixture by >7-10x** from 2-3 analytes if 6-10 very sensitive but semi-selective detectors were to be used alone, such as SAW or nano-cantilever detectors (limited by the availability of orthogonal adsorbing polymers) to above 20 analytes if the 10-200 independent elution time "bins" of a GC are added to the analysis
- **Reduced probability of false positives and false negatives by 3-16x** by leveraging the benefit of 2-to-3-dimensional analysis via the addition to a spectrometer of one to two multi-channel detectors (e.g. micro discharge and/or fluorescence, each of which count as a new measurement dimension with 4 detection "channels") in a different dimension. Such composite systems are facilitated by the small scale and cost of MGCs.
- **Further reduced probability of false positives by ~100x** if about 10 MGAs are networked, which would become prohibitively expensive if done with conventional size analyzers.
- **Reduced cost by 10-100x** of the detection system, based on the advantages of high-volume batch fabrication and assembly, and low materials costs.

In comparing alternate analyzer strategies to achieve the stated performance goals, especially in relation to the desired reduction in false positives, we classified analyzers into simple and composite categories. The "**simple detection**" approaches we considered are:

- A single spectrum analyzer with one non-selective detector, such as:
  - Non-dispersive optical absorption spectrometer w/a tunable laser as light source and a microphone/thermistor as detector
  - Dispersive optical emission spectrometer to record the output of a micro-discharge device
  - Mass spectrometer
  - Gas chromatography (GC or boiling point spectrometer) w/one non-selective detector
  - Ion drift or mobility spectrometer
- NDIR with several fixed-wavelength laser sources and one microphone/thermistor as detector
- Fluorescence and thermionic ionization detector
- Gravimetry (sensing adsorbed mass on a SAW and nano-cantilever)
- Photo-ionization detector (PID)
- Atomic emission detector (AED)

The **composite approaches** we considered are the same as the above but engaging two or more of them for each analysis. One powerful approach is to leverage the analyte separation power of a device like a GC "spectrometer" before the separated components are exposed to further analysis, i.e. leveraging multi-dimensional analysis and the number of effectively orthogonal measurements, to minimize false positives. The GC stands out among all other spectrometers in that, besides providing an elution time or "boiling point spectrum" of analytes in the gas sample, it facilitates further analysis of each individual analyte, and overcomes the many challenges of analysis of complex mixtures (masking of analyte response, combinations of interferents giving response similar to that of target analytes).

2. Competitive Position and Advantage of the Micro GC Analyzer

Examples of some recently published, highly sensitive and potentially competitive gas sensing approaches were checked to determine their relative chances of meeting the stated DARPA Goals. As shown below and despite their impressive features, they can only meet some of those goals:

- **NDIR: Tunable laser source w/optical or OA detection**: May achieve detection of 10 ppb C2H2 w/20 cm cell and ~10,000 internal reflections[3], but **cannot meet 1-10 ppt and 2 cm^3, especially when analyzing mixtures with complex backgrounds.**

- **Polymer-coated nano-cantilevers**, w/single molecule sensitivity[4,5] or resistive hot-plate sensors[6]: The power requirements of polymer chemi-resistors are in the sub μW range, but they are **unlikely to meet the P_{fp} of 1/2,500** (see Table 2 in Appendix D.5, first row). However, if their response time can be dropped from the 1-10 second range to ≤ 1 ms, they may become very effective and low-power μGC detectors

- **Ion Mobility Spectrometer**: May be a sensitive CWA detector but their **size (minimum of 6 cm in length) and sample flow rate needs to be reduced. IMSs tuned to detect broad CWA threats have false positive problems**

- **Macro-GC of Today vs. Micro-GC Pre-Concentration**: Today's pre-concentrators are too slow and use too much power to approach the stated DARPA goals. On the contrary, MGC-based preconcentration, as represented for example by 20-element PHASED approach, offers orders of magnitude advances towards the DARPA Goals.

Pre-Concentration Comparison between Macro and Micro GC

	micro-GC	macro-GC	Gain
-Collection time in seconds:	3-10*	100	>10
-Pre-Conc. Gain, N (for a single-stage):	N	N	1
-Total gain (20-100 stages):	20-100xN	N	20-100
-Size for multi-stage PC in cm^3:	0.1x1x0.5	0.6cmϕx10	>50
-Desorption time in ms, per stage:	< 5	~5000	1,000
-Desorption energy mJ:	2.2 mJ/stage**	10Wx5s	>10,000

---

* Gain x sample gas flush time; measured saturation in seconds

** Based on measured 0.44°C/mW (0.45 W to heat up to 200°C for 5 ms; 44 mJ for 20 stages)[7]

3. Estimation of Comparative False Positives. Modeling of the probability of false positives, P_{fp}, and its application to a few selected examples led to the following expression, derived in Appendix 5:

$$P_{fp} \sim 1 / [(1 - \exp\{ -(R_{SN} -1) / 4\}) (n_1 n_2 \cdots n_m)^{0.8} + 1],$$

where R_{SN} = S/N ratio and n = n_1, n_2, ... = the number of independent measurements each spectrometer or detector can make on the gas sample presented to it. This expression yields values of $0 \le P_{fp} \le 1$, with the most desirable one being as close as possible to zero. As the analyte signal disappears and R_{SN} drops from ~10 to 1, P_{fp} approaches the value of unity. However, values of $R_{SN} \ge 10$ do not further influence P_{fp}. The exponent z=0.8 represents an informed choice between the value of z=0.5 for random statistical processes to influence P_{fp} and z=1, which would represent an error-free, analytical solution to n unknowns related through n equations. Increasing the number of resolvable measurements of one spectrometer would **additively** increase the value of n, but introducing a new

measurement method or dimension with its own n_2 independent measurements would **multiplicatively** increase it.

To put this in perspective via some examples, it appears that individual spectrometers (NDIR, mass or GC), each with 100-1000 independent measuring "bins" or channels can achieve false positive probabilities (on a relative scale from 0 to 1) of P_{fp} = 1/37 to 1/226, but cannot match the low probabilities achievable by existing or imagined multi-dimensional analyzer systems, which might achieve P_{fp} < 1/2,500, or even below 1/288,000, by smart networking just 10 micro analyzers (see Appendix 5).

Selectivity and broad sensitivity to known and future analytes are conflicting attributes for direct or simple detectors. This conflict may be overcome by either:

- An array of parallel, individual and highly selective detectors, which would be dedicated to the detection of individual toxins or analytes, but would result in extremely costly and bulky detection systems, and most likely only unacceptable P_{fp} values due to lack of redundancy, or
- Separating the functions of **selectivity** (via the separating capabilities of spectrometers augmented by physically diverse detection technologies) and **sensitivity** (via pre-concentration plus optimal detector), which enables achieving simultaneous maximum S/N ratio for analyte detection and minimum P_{fp}.

Examples of detection approaches with increasing number of independent measurements and therefore also decreasing frequency of average false positives, are listed in Table 2 of Appendix 5, together with the results of preliminary ROC curve data (area above the curve.).

4. MGC Performance Simulation and Modeling. MGC Column Design Tradeoffs.

As stated in the Summary, this report is accompanied by a series of derived simulation models, so that the reader can use them as easy-to-use tools for evaluation of parametric sensitivity and tradeoffs. The four programs submitted with this report are:

M1 Gas chromatography column design/tradeoff model based on Golay's equation**.**
M2 Computation of the column's peak capacity
M3 Estimation of False Positives Fraction
M4 ROC (Receiver Operating Characteristic) curve analyses and calculations, and MGA comparisons

These four are enclosed in Excel format. All their inputs are highlighted in yellow.

These models perform the following functions :

Model 1. **Micro GC Parameter and Performance Tradeoff Simulation**, whereby a User can input values for the gas and stationary phase, column geometry and see the results plotted to the right, after exercising Solver (click cursor on D21) then press Solver in the Tools menu) to obtain the optimal flow velocity, v_o, and achieved maximum Resolution at v_o.
Double-klick on File TL-03-uGC-Model.xls

Model 2. **Determination of Peak Capacity** for 0.1 < k' < 5. This tool was intended to help with the determination of peak capacity vs. scaling. It is based on the simple summation of peak half widths along the time scale, until the maximum k' or maximum time has been reached. The desired scale factor (1-100x down from conventional GC practice) is the input. The output result is at the discretion of the user, being dependent on the agreed k' range, i.e. the associated boiling point range.
Double-klick on File TL-03-uGC-Model.xls

Model 3. **Estimation of the Fraction of False Positives** under idealized conditions
Inputs are R_{SN} and n, as marked on these two columns, into any row element.
Double-klick on File TL-03-False-Positives.xls

Model 4. **Calculation of ROC Curve Data**, incl. the area over it (representing instrument errors) from test results input data and from assumed data symmetries corresponding to various scenarios. The installed demo assumes that there is 1 error for the entered (=input!) number of tests. Also included is the Table (2) for comparing the performance of different gas analyzer approaches, including the GC-MS "Gold Standard".
Double-klick on File TL-03-ROC-Compare3.xls

5. Technology Hurdles
The hurdles we have listed in the above Summary presently represents our complete list.

6. DoD-Relevant Applications. The availability of MGAs or MGCs that meet the listed DARPA Goals will significantly advance the ability of deploying such analyzers in **military applications**, such as in ultra-light UAVs (Unmanned Air Vehicles) and air-deployed unattended ground sensing (UGS); additional DOD applications that parallel envisioned **commercial applications** would be their use in the fuel processing/petrochemical industries, environmental, quality and safety control, and medical breath diagnostics. This following, more comprehensive breakdown of DoD applications, was taken from Greg Frye-Mason's report, see Appendix D.2:

- Point sensor for remote detection
- Projectile or air-deployed (shoot or drop the MGA to the desired sensing location)
- Micro aerial vehicle sensors (10-20 mg payloads)
- Covert detection capabilities
- Sensor for perimeter protection/alarm for facilities or buildings
- Sensor for interior protection in ventilation of buildings or vessels
- Improved point sensors for present industrial, medical, environmental,...applications

7. Future Work. The contents of this report may serve to stimulate designers and researchers of MGA and MCG systems. Project teams which may be funded under DARPA BAA03-40 (full proposals due Nov.7, 2003), may find our short study report of use and as a source for design guidelines.

C. REFERENCES

1. DARPA Workshop on Micro Gas Analyzers, Monterey, CA, 16-17 December 2002
2. Ngai Wong, SBCCOM, Aberdeen Proving Ground, MD, Private Communications, Dec.'02 - Aug.'03
3. M.Gupta (Los Gatos Research), "Cavity-Enhanced Gas Analyzer for Process Control Applications," DOE-OIT S&A Annula Review Meeting, San Francisco, CA, 2-3 June 2003
4. Thomas G.Thundat (ORNL), "Better Detector for Plastic Explosives," Chem. & Eng. News, Aug.25, 2003, p.9
5. Panos Datskos (ORNL) datskospg@ornl (865) 574-6201, "Nanosensor Arrays for Chemical Sensing...", , http://www.ornl.gov/lasers_optics_diagnostics/FactSheets/CalSpecNEMSChembio.pdf;
6. Scott Nance (and Steve Semancik, NIST-CSTL), "Agency Developing Wearable Chemical Sensors," Defense Week, Vol.24, No. 38, p.1 and 14 (2003)
7. U.Bonne, PHASED Micro Analyzer", DARPA Workshop on Micro Gas Analyzers, Monterey, CA, 16-17 December 2002
8. U.Bonne (Honeywell Labs), G.Eden (U.Illinois), G.Frye-Mason (Nomadics, Inc.), C.Herring (Caviton, Inc.), R.Sacks (U.Michigan) and R.Synovec (U.Washington), "Micro Gas Chromatograph Tradeoff Study - Interim Report," to DARPA-MTO/AFRC/UTC for BAA N66001-03-X-6001, 25 Aug. 2003
9. JSLSCAD (Joint Services Lightweight Standoff Chemical Agent Detector), a small, fully-automatic, standoff chemical agent detector http://www.globalsecurity.org/military/systems/ground/jslscad.htm

D. IN-DEPTH REPORTS

1. **Photo-Detection and -Emission of MDDs by Gary Eden, U. Illinois and C.M.Herring, Caviton Inc**
2. **MGC Detector Requirements by Greg Frye-Mason, Nomadics, Inc**
3. **Parametric Analysis of MGC Column Performance by Richard Sacks, U. of Michigan**
4. **High-Speed Micro-GC Performance and Chemometrics by Rob Synovec, U. of Washington**
5. **Derivation of a False Positives Model for MGA Comparisons by Ulrich Bonne, Honeywell**
6. **Capabilities of Laser-Based Optical Absorption Approaches by Ulrich Bonne, Honeywell**
7. **Ion-Drag and Fluidic Diode Pumping Approaches, by Ulrich Bonne, Honeywell Labs**
8. **Miscellaneous Information**

1. Photo-Detection and -Emission of MDDs
by Gary Eden, U. Illinois and C.M.Herring, Caviton, Inc, 5. Sep. 5, 2003, rev. 19 Nov. 2003

The University of Illinois/Caviton, Inc. portion of this Project Team is focusing on the unique properties of microdischarge devices (MDDs) and their potential impact on a micro-gas chromatography system. We are exploring MDDs both as emitters and sensitive detectors with the sole goal of realizing a novel, ultra-sensitive chemical detection system.

A. Photodetector Experiments and Calculations

Although time constraints do not permit extensive experimentation in this study, we have conducted initial experiments to ascertain the sensitivities of MDD photodetectors because of their small size (nanoliter Æ picoliter volumes) and ability to be integrated with other Si electronics. **Figure 1** shows the results of preliminary experiments in which the photosensitivity of microdischarge devices, having an aperture of (100 μm)^2 and a Si photocathode, was measured in the visible and near infrared. When operating with 500 Torr of Ne, these devices exhibit sensitivities of up to 3000 A/W, or almost two orders of magnitude larger than that of the best commercially available Si avalanche photodiodes (APDs). The spectral profile for the detector is similar to that for conventional semiconductor photodetectors, suggesting that the photoresponse is, indeed, determined by the Si photocathode. It must be emphasized that we have only tested these devices with Ne - other gases or vapors will almost certainly increase the sensitivity of the device.

In order to assess the utility of these photodetectors for chemical detection, measuring the detection "floor" is critical. These studies are in the early stages but we have already measured incident power levels of ~5 nW without synchronous detection. It already appears that this device will be capable of reliable photodetection at the pW level or below (corresponding to ~10^7 photos/sec in the visible and UV). Furthermore, the detectivity (D*) of the detector has been estimated to be comparable to that of the human eye. This is a remarkable result for a non-vacuum device operating at room temperature. The photosensitivities cited above are to be compared with the "gold standard" in photodetectors, the photomultiplier, which has a maximum sensitivity of ~10^5 A/W. However, the photomultiplier is, of course, a vacuum device and has a very limited dynamic range.

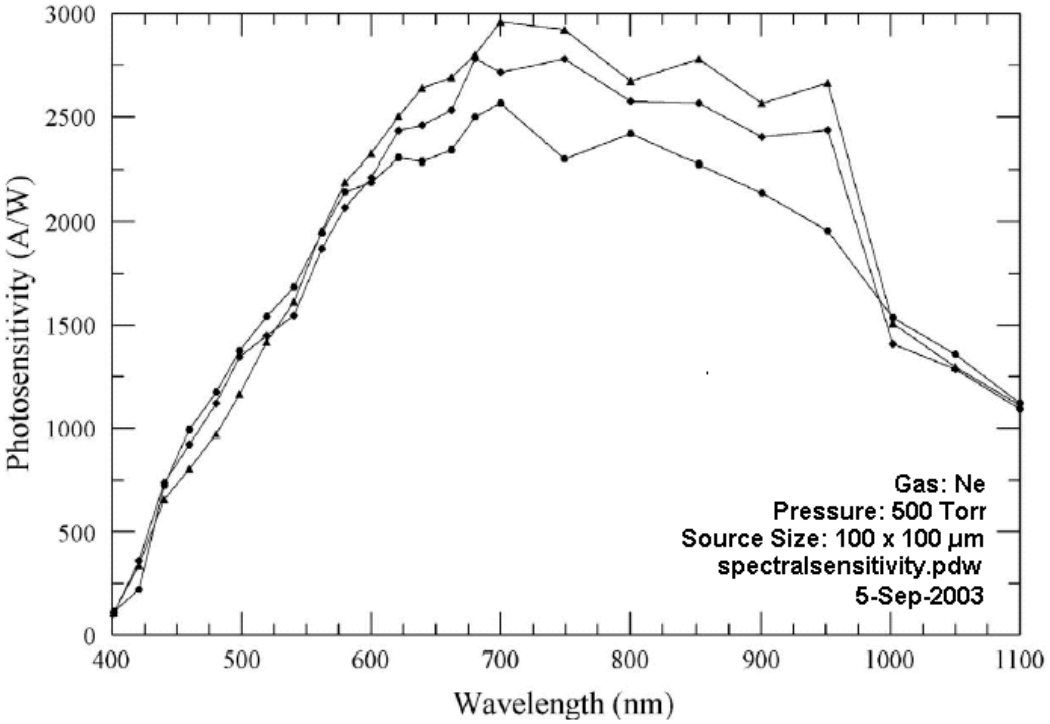

Fig.1. Spectral Sensitivity of MDDs at Ambient Temperature for 3 Fab Runs

On the basis of our study to date, the MDD photodetector appears to be an "enabler" for a completely new generation of chemical detection system. When coupled with another MDD to generate the emitting atomic or molecular species, it appears to be quite possible to reliably detect trace emitters. For example, a number density of only 10^{10} cm^{-3} (~10^{-6} Torr) of an emitting species having a (long)

radiative lifetime of 1 μsec will generate 10^9 photons/sec from a volume of 100 pL, or more than two orders of magnitude above our current estimate of the detection floor. When combined with a μ-GC "front end," the effective sensitivity will be increased by several orders of magnitude. This bodes well for integrating one MDD (or an array) into the same Si structure housing other components and realizing unprecedented sensitivities from picoliter volumes.

B. Photoemission from an MDD

An MDD is also a versatile and powerful emitter for chemical element detection and experiments are underway to provide data valuable for estimating detection floors. The experiments are pursuing two avenues for obtaining strong emission (and, simultaneously, information regarding chemical bonding) from the desired chemical agent. The first is directly exciting the agent in the MDD itself. Electron impact excitation or dissociation produces emission from the species itself - or one of its fragments. Another advantage of an MDD is that it operates at specific power loadings no lower than tens of kW per cc, up to as high as hundreds of kW per cc. These values are unprecedented for macroscopic devices on a CW basis and suggest (as we have already seen) that atomic radiating species will be produced, even from the most strongly bound chemical species.

A second avenue we are pursuing is to use the MDD to produce a vacuum ultraviolet (or extreme UV, XUV) emitter that will photolyze the molecular agent and produce readily-detectable fragments (molecular or atomic).

In summary, the MDD offers the ability to produce atomic or molecular fragments from the "parent" chemical agent molecule by electron impact in the actual discharge or by photolysis with 6-12 eV photons produced efficiently by the MDD. One emitter that can be implemented immediately is the Xe_2 molecule that is efficiently (h >10-20%) produced by an MDD. The radiating wavelength is 172 nm, corresponding to a photon energy more than ample to dissociate most polyatomics. Actually, both could be done in the same μ-GC system since the MDDs can be made as small as 10 μm (currently). We believe that obtaining both sets of spectral data simultaneously will increase dramatically the sensitivity of the detection system and improve the ability to make more rapid identification of the agent itself.

C. Photo-Emission of MDDs,
by Cy Herring, Caviton, Inc., 23 October 2003

Another task of the study was to estimate the extent to which molecules could be spectroscopically identified as they enter the microdischarge device. Typical operating power densities of the discharges are several 10's of kW/cc, and atomic transitions have been identified of He^+ with upper state energies in excess of 75eV above the ground state of neutral He. At these energies and power densities, most complex molecules are broken apart in the discharge, and emission is observed only from the atomic and molecular fragments from the parent molecule. However, each molecule that enters the discharge produces different relative concentrations of molecular fragments, which in-turn produces emission spectra that serve as molecular identification.

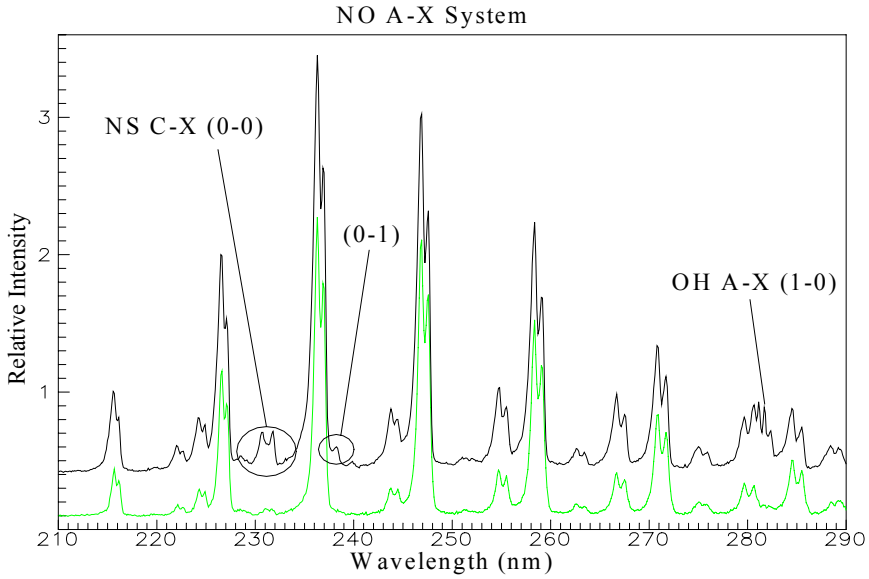

Figure 2. Spectral data showing evidence of sulfur (as NS) in a nitrogen-rich discharge. Upper trace shows a spectrum of nitrogen containing 62ppm SO_2, and the bottom trace (green) shows a spectrum of nitrogen containing 23ppm NO.

Additionally, some molecules have an additional atom/molecule to serve in identification such as arsenic, phosphorous, and sulfur, which are found in many CWA's.

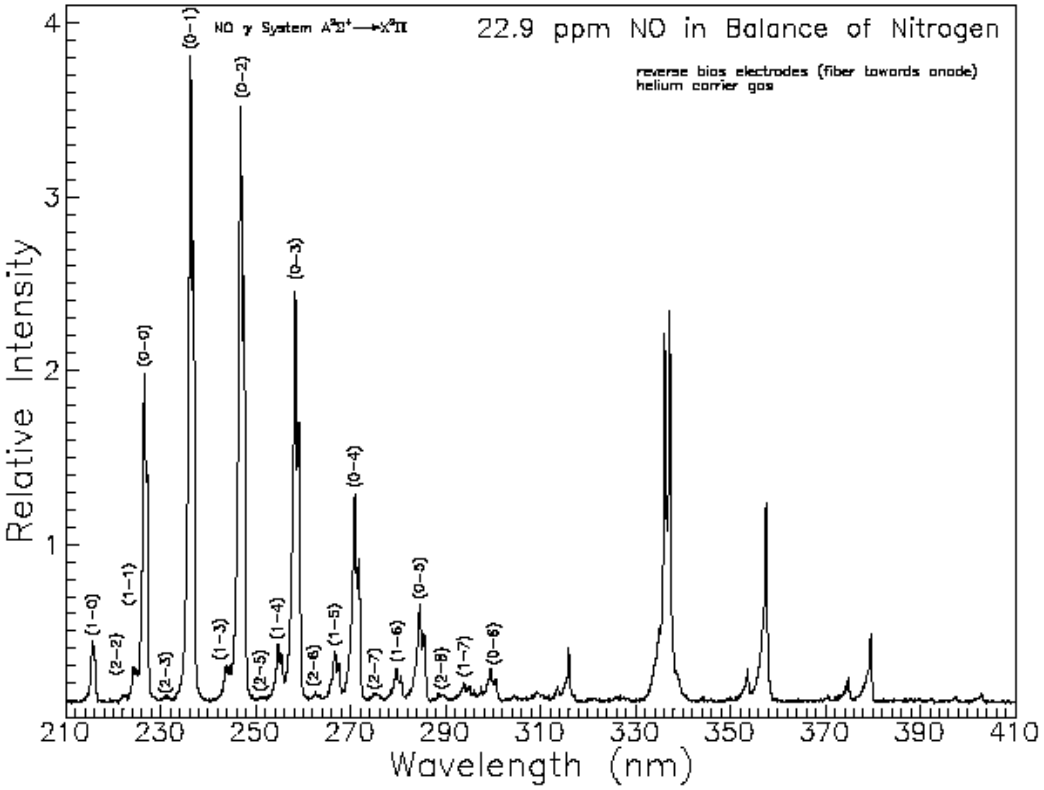

Fig. 3. MDD Emission Bands of NO, for a Discharge with 22.9 ppm NO in N2

The ultraviolet region of the spectra provides the greatest region for detecting diatomic molecules, and microdischarge devices have produced spectral emission from molecules identified as NO, CO, NS, CN, CH, N_2, OH, PO, NH as well as atomic emission from a number of elements. Figure 2 shows emission spectra between wavelengths of 210 and 290nm. Two spectra are shown, one of nitrogen that contains 23ppm NO, and another of nitrogen that contains 62ppm SO_2. The largest peaks seen in this region are due to NO, but there are several key differences noted in the figure. The upper spectrum of the gas containing SO_2 shows peaks due to NS in addition to an OH peak. The OH peak is likely due to different moisture contents of the two gases, but the NS is a product of the reaction of SO_2 with N_2 in the discharge. Spectral signatures such as these can be used to identify molecules containing sulfur, and a similar principle would be used for other molecules. Close inspection of the spectral peaks in Figure 2 show two small peaks due to NO at wavelengths 230.95 and 231.63nm, which lie close to the NS peaks at 230.52 and 231.72nm and the NS peak at 238.36nm is on the shoulder of a strong NO peak at 237.02nm. The NO band identities from emission observed and recorded with an MDD are marked in Fig.3.

.The initial tests show that it is possible to use molecular excitation spectra to identify chemical species that enter the discharge. We expect that modifications in discharge geometry and power delivery can be used to selectively excite species

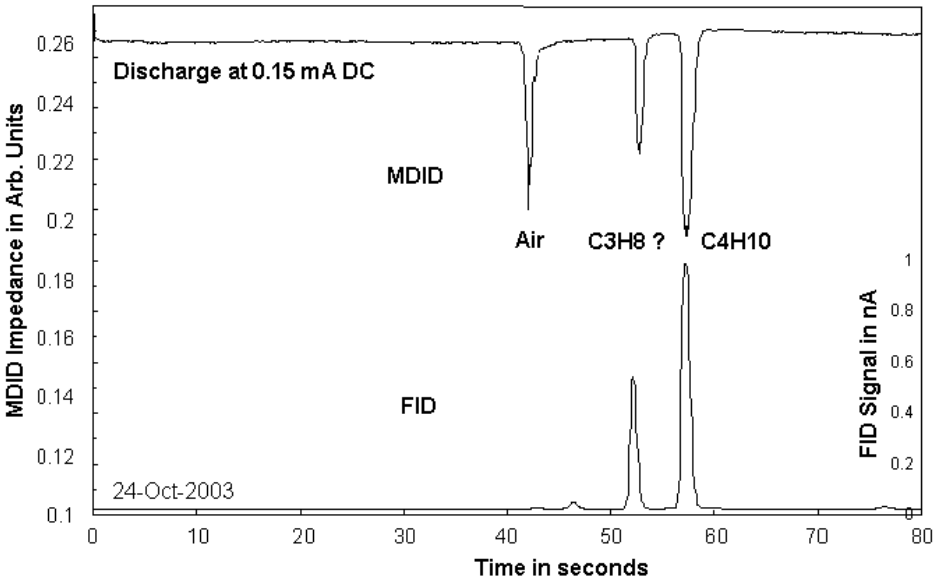

Fig. 4. First MDID Analysis of a Butane Lighter Gas Sample in Air, with an HP 5890 GC, Compared to FID Signals Blind to Air. He Carrier, 10 m, 100 µm, RTX1, 35°C Courtesy of C.Herring, Caviton, Inc.

of interest and to improve the S/N for trace quantity detection for not only sulfur, but other compounds as well.

MDIDs, Micro Discharge Impedance Detectors: As soon as GC-separated analytes from the sample gas enter the plasma of an MDD, the microdischarge will generate measurable:

- IR, vis and UV emission spectra representative of their composition, as discussed above,
- Ions and electrons which will readily attach to other molecules such as O2 and CWAs, and
- Changes in the MDD impedance, i.e. the basic effect used for MDIDs.

Caviton's preliminary characterization of MDDs and MDIDs have shown that sensitivities comparable to FIDs (GC flame ionization detectors) can be easily achieved by monitoring the potential applied to the discharge device, see Fig. 4, which shows that the MDID can detect an "air peak" in a He carrier gas stream that the FID cannot and is not expected to detect.

MDDs as GC detetors have also been under development at LLNL, as evidenced by Conrad Yu's publications and patents[1,2]. They found that MDDs (CW glow discharge controlled through a biased resistor) in a He carrier gas "can detect the change of electron density caused by impurities in the He carrier gas by many orders of magnitude larger than that caused by direct ionization or electron capture"[1].

References

1. Jackson C.Koo, and Conrad M.Yu (LLNL), "Glow discharge detector", U.S.Pat. 6,457,347, 1 Oct. 1999, assigned to The Regents of the University of California
2. Conrad Yu et al, IFPAC 2001

2. MGC Detector Requirements

by Greg Frye-Mason, Martin Leuschen, Marcus la Grone, John Sikes, and Eric Towers,
Nomadics, Inc., October 31, 2003

Introduction

This report focuses on issues related to critical performance requirements for MGC detectors and specifically discusses several detector options and their advantages and disadvantages related to meeting DARPA's challenging performance requirements. It also includes some discussion of the ability of MGC systems to provide low false alarm rates based both on modeling and data from Sandia's'µChemLab™ system. Finally, it briefly discusses pumpless flow designs and DoD applications enabled by MGC systems.

A: Critical Performance Requirements for MGC Detectors

1. **Rapid Response**

- Low millisecond response times are required to obtain the sharp MGC peaks for three-second separations.
- Fast response times are required of all analytical components, all associated data acquisition electronics, and the data processing needed to get chemical identification. Note: mass spec or IR analyzers will likely not be applicable in full spectrum mode since they will be unable to provide full spectrum fast enough. Even if this were possible, the microsystem would not have the processor/memory power to handle data with the few second analysis goal.
- Rapid response must be achieved with a very low flow rate:
  - Modeling was done using the modified Golay equation (1) to optimize columns for Sandia's µChemLab™ technology based on 6 psi vacuum from pump and 1 m column. This showed that for the rectangular columns being used, the optimal width was 40 micron and the flow rate was about 0.2 cm^3/min for N_2 or air (optimal for H_2 is wider with flow rate about 0.8 cm^3/min showing one advantage of H_2 over air or N_2).
  - To reduce from 30-60 seconds to three seconds will require even smaller columns and consequently, flow rates will likely decrease by an order of magnitude (0.02 cm^3/min for N_2 and 0.08 cm^3/min for H_2)

As shown in Table 1, flow rates can have a significant effect on both preconcentrator and detector time constants. This indicates a need to consider speed at low flows in selection, design, and development of preconcentrators and detectors.

2. **Chemical Selectivity/Discrimination**

- As highlighted by modeling on false positive rates (described elsewhere in this report), detector selectivity is critical to achieve very low false positive rates and high true positive rates.
- There are two components to detector selectivity that must be considered for evaluating detectors for a particular application such as detection of CWAs:

Table 1: Effect of flow rate on time constant for microfabricated preconcentrator and surface acoustic wave (SAW) array detector.

Preconcentrator		Preconcentrator / SAW Sensor		
Flow Rate mL/min	FWHM msec	Flow Rate mL/min	FWHM msec	Peak Height
6.5	50	35.6	1400	14
1.9	250	3.5	1800	37
1.1	470	0.5	17,000	17
0.6	1250			
0.3	2700	FWHM = Full Width at Half Max		

The preconcentrator is a 2.5 mm square SiN membrane with integrated heater and a thin sol-gel adsorbent film. Testing was performed in an HP 6890 GC using dimethyl methyl phosphonate (DMMP) in the carrier gas and observing the peaks upon thermal desorption using the flame ionization detector in the GC. The SAW devices are 510 MHz devices with an active area of 300 x 800 µm. DMMP was collected on a microfabricated preconcentrator and then desorbed onto the SAW array at various flow rates.

Data presented at Dec. 2002 workshop and used courtesy of Sandia National Labs.

- First is the number of orthogonal measurements (n_1), an indication of how much chemical information is provided. Detectors tend to fall into three classes:
    - High selectivity with n_1 = 100-1000 (e.g., mass or optical spectrometers; only this high when a full spectrum is obtained)
    - Modest selectivity (class selective, arrays) where n_1 is typically from 3-10
    - Limited or no selectivity (TCD, FID) where n_1 is 1
- A second important factor is related to how well the detector is tuned to preferentially see the target analytes from the much larger set of potential interfering analytes that may be present in the background. For some detectors, the device may only detect a small fraction of the chemicals present and have little or no response to other analytes. For other detectors, there may be enhanced detection of the target analytes so they are easily discriminated from most background species. An example here would be hydrogen bond acidic materials for acoustic sensors that provide an enhanced detection of nerve agents, enabling them to be discriminated from typical backgrounds easily (even though n_1 is only 3-5).
- **Discriminating Power**, $n_1 \cdot n_2$. A parameter that can be multiplied by n_1 to get the total discriminating power of a detector is n_2 = (total number of chemicals potentially in background)/(number of these chemicals the detector is sensitive to) = 1/(fraction of species detected). While there is a strong need to drop the false alarm rates of current detectors for CWAs, the two main technologies currently in use are as effective as they are because of this effect.
    - Ion mobility spectrometers have very poor resolution. In fact, if one looks at the peak widths and the range of drift times and compare this to GC separations, it is found that n_1 is low and sometimes only about 5-10. However, using a reactant gas that will pull ions from a large percentage of the background analytes but will give up the charge to highly active analytes such as explosives and nerve agents, these target analytes can be seen even in the presence of background analytes. For an IMS, n_2 is estimated at 50-100 for explosives and nerve agents (somewhat less for blister and blood agents since these are not as active in collecting charge) so that $n_1 \cdot n_2 = n_{IMS} \sim 500$.
    - SAW sensor arrays take advantage of a decrease in sensitivity with increasing volatility so that many volatile analytes such as gasoline fumes or solvents are poorly detected and from the use of selective materials that provide response patterns (especially for nerve

agents) that are very distinct from other analytes. For a SAW array, n_2 is estimated at 50 to 100 so n_{SAW} ~ 250.

- This second factor in discrimination also should be considered with the sample preconcentrator since the adsorbent material and amount can be tuned to effectively collect and concentrate the target analytes but not concentrate to any significant extent a large amount of the background, especially more volatile agents. Using this combination of effects results in an almost total insensitivity to volatile organics such as toluene in the current Sandia μChemLab system (no peak seen even at > 1000 fold higher concentration than CW simulant even though toluene does go rapidly through column as sharp peak). If one estimates n_{PC} ~ 10, then $n_{PC\text{-}SAW}$ ~2500, even without a GC column. This number being higher than for an IMS is consistent with the fact that SAW arrays tend to have an advantage over IMS sensors in providing fewer false alarms.

3. **Very High Sensitivity**

We list below some estimates regarding the analyte flux and total amount of analyte that needs to be detected as a function of various detection limit targets.

- Sensitivity is driven by the fact that the volume of gas that can be collected in a short period of time is very small. In addition, even if it was possible to collect from a larger volume, the collected analyte would overwhelm the microscale GC column.
- It is estimated that the volume of gas collected for each maximum sensitivity analysis will be in the range of 0.1 to 1.0 mL. This is based on sampling rates of 5-30 mL/min and sampling times of 1-2 seconds to meet the target analysis time of 4 seconds.
- This can still represent very large concentration factors since the volume being desorbed into is equal to the flow rate times the peak width. If one assumes 0.2 mL/min and 30 msec, then this is 0.0034 mL/sec * 0.03 = 0.0001 mL or 100 nL. This gives a concentration factor of 1000 for 0.1 mL collected and 10,000 for 1.0 mL collected. Flow rates and peak widths may be even lower.
- The amount of analyte and the rate of analyte assuming a 30 msec peak width are shown in Table 2 as a function of the two sample volumes and a range of concentrations down to 1 ppt.

Table 2: Amount of analyte available for detection by an MGC detector and the rate of analyte flux. Values assume a 30 msec peak width (triangular peak with 30 msec full width at half max) and a molecular weight of 150 g/mole.

Volume Collected (mL)	Concentration (ppb)	Analyte Mass (pg)	Molecules (billions or x10^9)	Analyte Flux (pg/sec)
1	10	61	260	2050
1	1	6.1	26	205
1	0.1	0.61	2.6	20.5
1	0.001	0.0061	0.026	0.2
0.1	10	6.1	26	205
0.1	0.001	0.00061	0.0026	0.020

- The amount of analyte is very small compared with what is analyzed using current bench top instruments. Low femtogram detection is required for MGC. With typical current systems, low picogram detection is good.
- For sensors that generate a signal related to the rate of analyte (such as ionization or emission detectors), the pg/sec rates are comparable to what is detected using current bench top

instruments (push limits at very low end of range but only by about an order of magnitude or two). The sharp pulse significantly helps compensate for the small amount of analyte.

4. **Other Requirements**

- **Size:** Clearly to meet the 2 cm^3 goal for the whole system, the detector and associated electronics must be very small, ideally a few tenths of a cm^3.
- **Power:** Since the target will be 1 J/analysis or less, the detector must be low power. To meet the 1 J/analysis for four seconds means have 250 mW total so detector needs to be less than 100 mW and ideally less than 10 mW (especially for multiple detectors and channels).
- **Simplicity:** To make the whole system simple to fabricate and assemble, simpler detectors with fewer independent components and ones that are easy to integrate are preferred. In addition, simple data output and data analysis are important to enable the system to be operated and the data analyzed with the minimal microprocessor and memory capabilities that can be incorporated into the 2 cm^3 system.
- **Minimal Support Requirements:** Requirements such as special carrier gases with some detectors, high vacuum operation for MS, and other support features need to be considered. In some cases such as MS, developing miniature components to meet the support requirements is much more difficult than developing the detector and may rule out the detector as an option for an MGA.
- **Cost:** The ability to fabricate and assemble the detector at low cost is an advantage but is not critical for all applications.

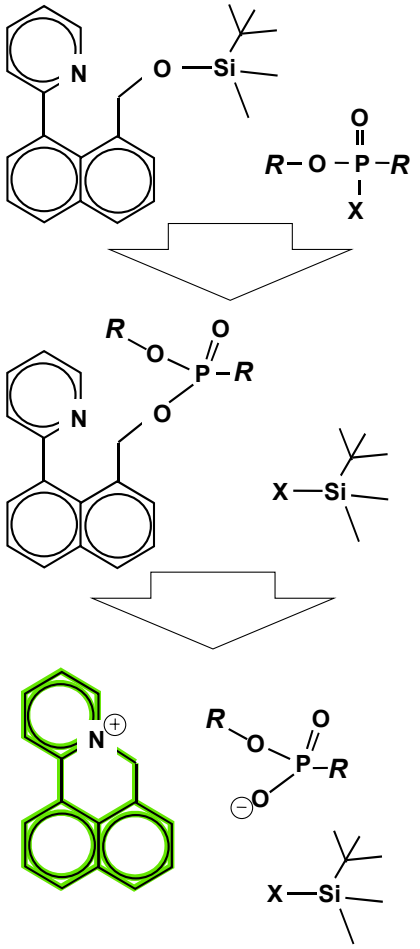

Initially, the compound is not fluorescent in the visible range. However, after the nerve agent strips off the silane it cyclizes into a fluorescent conjugated ring structure.

Figure 1. The CWIC (left) reacts with a nerve agent (right).

B: Ability of Selected Detectors to Meet MGC Requirements

1. Fluorescent Detectors

This is a new class of detector under development at Nomadics (2). It is based on a fluorescent, chemical- weapon-indicating chromophore (CWIC) developed recently by Professor Timothy Swager of the Massachusetts Institute of Technology (3).

- CWIC (normally not fluorescent in the visible range) reacts with most CWAs and several TICs to produce a highly fluorescent compound that can be easily detected (Figures 1 and 2).
- System components include a CWIC coated substrate, an excitation source such as a UV LED, a photodetector, and appropriate filters for each. High miniaturization potential.
- It is extremely sensitive. Figure 3 shows a two-second response to 15 ppb diethyl chlorophosphate (a weak organophosphate nerve agent) giving a S/N (Signal/Noise Ratio) greater than 3000 (Figure 3). Sensitivity is enhanced by the dark field nature of sensor – the lack of ambient light (in the emission band of reacted chromophore) makes very small signals very obvious.

- It offers a high-speed response:
  - Steep part of curve at 15 ppb exposure in Figure 3 gives S/N=10 in 20 msec (the 15 ppb concentration used in this figure could be generated from 1.5 to 150 ppt after 100-10,000 fold preconcentration)
  - Higher concentrations lead to steeper slopes (S/N of 10 in 3 msec has been shown at 100 ppb) so higher concentrations and preconcentration decrease response time significantly

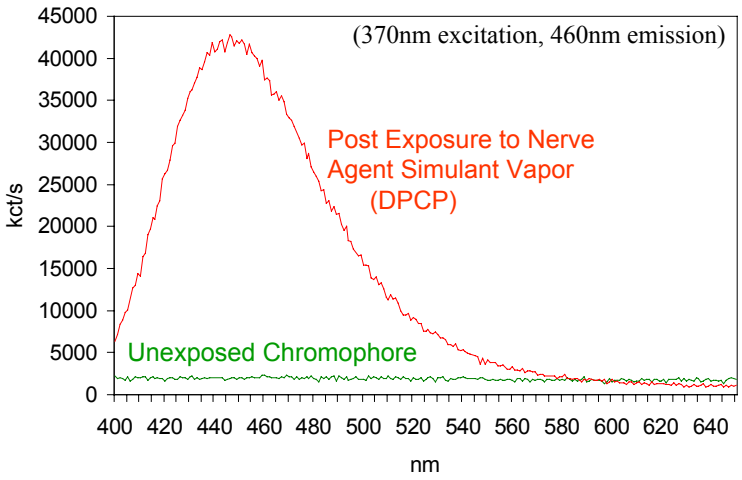

Figure 2: Reaction of a nerve agent surrogate with the CWIC converts if from a nonemissive form to a highly emissive chromophore.

- It has focused selectivity:
  - Unique reaction based detector only sees active species (no response to non-reactive simulants like DMMP). For a single film, have n_1 = 1 but have n_2 > 1000 since only a small number of toxic and reactive species generate a response. In fact, for applications where it is desirable to detect TICs, this value is even higher since it takes a toxic chemical to generate a response.
  - CWIC will detect nerve agents (GA, GB, GD, GF), choking agents (CG and DP), and blister agents (HL and Lewisite).
  - Will detect several chemically active TICs and CW precursors such as $SOCl_2$ and concentrated acids.
  - Ability to detect VX and the mustard agents HD and HN currently under development. HD simulant detection in solution is already reliable.
- Sensitivity calculation for trace detection verifies sufficient sensitivity to meet MGC detection needs:
  - For 50 µW incident, we estimate 60 fW auto fluorescence, based on data with current systems and scaling the size and thickness of the substrates
  - Estimate 60 femtogram active agent should give 2.6 pW which would provide a signal/background = 50 and a signal/shot noise = 2500.
  - This assumes 10% conversion efficiency, 30% optical capture efficiency, 80% filter efficiency, and one photon emitted per second per chromophore

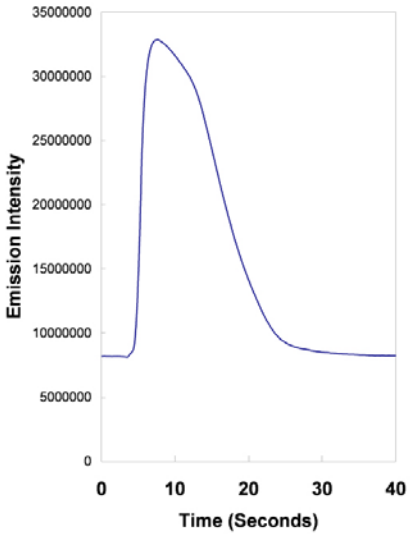

Figure 3. Demonstration of large S/N detection of a reactive G-agent simulant for a two second exposure at 0.1 mg/m^3 (15 ppb). 370-nm LED excitation and detection with a photomultiplier tube (PMT) and a band pass filter (360 nm center and 60 nm width).

2. Thermionic Ionization Detector (TID) and related detectors

This class of detectors uses a heated surface to generate thermal electrons. This surface typically contains an alkali glass bead, which facilitates emission of electrons, which preferentially attach to and thus selectively ionize CWA and other analytes.

- Typical reaction volumes are 0.5 ml. This can be scaled down along with the catalytic bead.
- Detectors tend to draw 2-5 W of power. 99% of this is to perform resistive heating of the bead; as the bead shrinks so will the power requirements (similar to advantage seen for sample

preconcentrators where 1000-10,000 fold power reductions achieved). Properly designed, the waste heat from the bead could be used to heat an isothermal column.

- The sensor is fundamentally robust. By minimizing H_2O exposure, one can expect a bead to last from months to years.
- A simple, classical electrometer is all that is needed to transduce the signal. Even "advanced" systems do not require high voltages or complicated timing sequences.
- NPDs (nitrogen phosphorous detectors) require H_2 for reaction chemistry. The volume of H_2 required scales with the system. H_2 is already desirable as a carrier gas.
- The selectivity can be varied based on the catalytic bead and operating conditions such as temperature and the gas used. For example, using nitrogen have nitro selective detection good for explosives and with hydrogen-air have selectivity to N and P containing analytes. This is good for many CWA agents including G agents that contain P and sometimes N, V agents that contain P, nitrogen mustards that contain N, and blood agents that contain N. TIDs in conjunction with NPDs would further increase selectivity. Fundamentally, the only difference between an NPD and a TID is surface composition and the need for H_2. The mechanical and electrical design is largely the same.
- These detectors can be very sensitive: <0.06 pg/sec N (~0.6 pg/sec for N containing analyte). For a typical MGA, this is equivalent to sensitivities to ambient environment concentrations of 3-30 ppt, depending on the volume of the initial sample collected and the peak width (e.g., 1 mL at 3 ppt into a 30 msec wide peak).
- Miniaturization and integration may enable lower noise levels or improved ionization efficiencies to provide even lower detection levels that should meet MGC requirements.
- Example of advantage of mole/time detector is shown in Table 3.

Table 3: Expected signal levels for an ionization based detector as function of analyte concentration assuming a molecular weight of 150 g/mole and a peak width (FWHM) of 30 msec (see Table 2 for comparison).

Volume Collected (ml)	Conc. (ppb)	pg/sec	Billions of molecules / sec	pA if 1% ionized and detected
0.1	10	205	861	515
0.1	1	20.5	86	52
0.1	0.1	2.0	8.6	5.2
0.1	0.01	0.20	0.86	0.52

Even with current ionization detectors, noise levels less than a pA are commonly achieved.

3. **Gravimetric or Acoustic Sensor Arrays**

- These sensors scale well with miniaturization (4), as highlighted by the data in Table 4.
- An example of this type of device is the 2.5 GHz thin film resonator currently made by Bill Hunt at Georgia Tech.
- The Sauerbrey equation for detection level (f_o is unperturbed frequency) is:
  - $\Delta f / f_o = - 2 * f_o * (\text{mass/area}) / (\text{shear modulus} * \text{density})^{0.5}$
- As linear dimension (h) is decreased, the area goes as h^2 and f as 1/h, so response to mass goes as $1/h^3 = h^{-3}$.
- Question: Can sorption based sensors such as microcantilevers or acoustic sensors be fast enough?

- Response time as h^2 since film thickness tends to scale as h.
- Elastomer diffusivity typically 10^{-7} to 10^{-8} cm^2/sec.
- 100-nm film, equilibration times of 1-10 msec.
- 10-nm film, equilibration times of 0.01-0.1 msec.
- Conclusion: can meet need with thin, fast diffusing films.

- Question: Are sorption-based detectors redundant with GC Column?
  - Function of coatings on GC and detector differ.
    - GC coating to separate from each other, generally based on volatility not chemistry (common nonpolar phase called boiling point column)
    - Arrays utilize multiple coatings with different chemical properties to probe the analyte chemistry.
    - Alkanes separated on GC result in the same array pattern.
    - Coeluting analytes result in different array responses.
  - There are a variety of orthogonal coatings that probe chemical properties and only one on GC. Some of the most selective such as hydrogen bond acids for nerve agents are not effective as GC phases due to a limited number of active sites, resulting in retention times depending on the amount of analyte.
  - Case in point: Sandia's μChemLab uses a GC/SAW array and it achieves good performance for discrimination and false alarms.

Table 4: Effect of miniaturization on mass detection of acoustic devices.

fo	Width (cm)	Area (cm^2)	Noise (Hz)	Mass (pg) for S/N = 10	
5.0E+06	0.5	0.2	0.2	7155	7 ng
2.5E+09	0.001	8.1E-07	100	5.72E-05	57 attog

Comparison of a 5 MHz quartz crystal microbalance to a microfabricated analog device, a 2.5 GHz thin film resonator. Even though noise scales with frequency, 500 fold frequency increase results in $(500)^3$ or 125,000,000 fold decrease in the mass detection level.

C: Role of Preconcentration, Separation, and Detection in Reducing False Alarms

- False Positive/Negative Rates - Advantage of Separations-Based System
  - For an analyzer that works well, false positives are almost all due to the presence of chemical interferents that look like a target analyte.
  - Complex interferents like gasoline, diesel, and exhausts contain many analytes. Consequently, there is a high probability that they may look like a target analyte.
  - Background interferents are a major factor for false negatives due to the masking of target analytes or a combined target analyte/interferent response that does not look like a target analyte.
- False Positive Rates - Advantage of Separations-Based System or μGC Concept

  In defining the probability for false positives as $P_{fp\text{-}\mu GC} = P_{fp\text{-}sensor} * P_{pc} * P_{complex} * P_{GC}$ where
  - $P_{fp\text{-}sensor}$ is the probability of an interferent that gives a detector response similar to a target analyte being present (this is typically low, ~0.01-0.0001; this factor should be considered for other analysis)
  - P_{pc} is the probability that the interferent above has a low enough volatility to be collected and a high enough volatility to be released quickly by the preconcentrator (typically 0.2-0.4).

- $P_{complex}$ is the probability an interferent not discriminated by preconcentrator is a complex mixture that is spread out by the GC so that no peaks are detected (typically 0.6-0.8) and
- P_{GC} is the number of target analytes to be detected that look similar to the detector (typical is 2-6) divided by the number of independent time windows in the GC trace (typical is 30-50), resulting in $1/25 \leq P_{GC} \leq 1/5$

We can now quantify the decrease in false positives by a μGC concept relative to that of a lone detector as the factor $P_{pc}*P_{complex}*P_{GC}$, with a best case of 0.2*0.6*(2/50) = 0.01 and worst case = 0.4*0.8*(6/50) = 0.064. Additional insights are:

- False positive rate decreased 15 to 100 fold by the addition of a μGC
- Increase $P_{fp\text{-}\mu GC}$ from one in 150 hours to one in 2300 to 15000 hours, meeting desired specification from Ngai Wong for point detectors (5).
- Similar analysis can be performed for false negatives.
- P_{GC} is now related to number of interferents in background that in GC separation window divided by the number of independent GC time windows.

- Field demonstration of advantages of using selective preconcentration, separation, and detection to provide very low false alarm rate detection.
  - Sandia's μChemLab CW detector has been placed into both the San Francisco Airport and the Boston Subway for testing over extended periods of time (6).
  - 70,000 runs with zero false alarms in the airport and now over 150,000 runs with ZERO false alarms in the subway.
  - 2 minute analyses continuous so 7300 hours or 300 days
  - Significantly better than target of 1:1500 hours and close to demonstrating goal of 1:288,000 analyses (5).
  - System was placed in a temperature controlled box measuring 14" x 16" x 8"
  - DMMP internal standard system in box to verify working and that would have detected an agent if it was present
  - Some drift issues due to GC fluidic connection and filter clogging in the airport test that appear to be solved in the subsequent subway test

D: Pumpless Design Concepts

There are various flow control issues and ideas to be considered. Regarding convection and diffusion scaling laws the main considerations are as follows:

- Convection and Micro Are Poorly Compatible:
  - Drawing samples through small bores is progressively more difficult as the dimensions of the system decrease. For a constant pressure drop through a bore of radius *r* and length *L*, the volumetric flow rate is proportional to r^4/L and the total drawn volume after a time *t* is $r^4\ t/L$. Thus, when the dimensions are reduced by a factor of 2, the flow rate is reduced to $(1/2)^4/(1/2) = 1/8$ as is the volume drawn in a given time. Therefore the ability of a small device to quickly draw analyte from a sample volume in a given time decreases very rapidly as the device dimensions are reduced.
- Diffusion/Permeation and Micro Work Well Together

- Diffusive transport through a permeable membrane of area *A* and thickness *h* in time *t* will interrogate a total volume proportional to $A\sqrt{t}/h$. Thus, when the dimensions are reduced by a factor of 2, the volume interrogated in a given time is reduced to $(1/2)^2/(1/2) = 1/2$. Therefore the ability of a small device to diffusively interrogate analyte from a sample volume in a given time decreases less rapidly than convective interrogation as the device dimensions are reduced. Further, the time for the concentration in the membrane to reach equilibrium with the sample is proportional to h^2. Thus, the time for the membrane to equilibrate decreases to $(1/2)^2 = 1/4$ and is therefore not limiting the uptake rate.
- Diffusion faster for absorption based detectors. Since diffusion equilibration times are proportional to h^2, when dimensions are cut by 2, equilibration times are cut by 2^2 or 4.

Pumpless design issues are as follows:

- Diffusive sampling onto preconcentrator.
  - By the Noyes-Whitney equation, with *A* the area of the membrane, *D* the coefficient of diffusion of the analyte, ρ the membrane porosity, and *h* the thickness of the membrane, we see that the mass uptake through a porous membrane to a preconcentrator is proportional to $A\ D\ \rho\ /\ h$. For example, a $1mm^2$, 40% porous, 40μm thick membrane allows uptake of an analyte with diffusion coefficient $0.1cm^2/s$ proportional to $1mm^2 * 0.1cm^2/s * 0.4 / 40\mu m = 0.1cm^3/s$. Thus, the target uptake of 0.1mL is achievable in 1s and 1.0mL in 10s.
  - With a pump/vacuum source for GC (low flow, high vacuum), can simply desorb and send on to GC.
  - For carrier gas design, a flap valve is needed to close off the membrane so the sample can be pushed onto the column.
  - Since the volume of the GC is extremely low, the total volume of carrier gas required to move analyte from the preconcentrator to the detectors is extremely low. This recommends the in-place generation of tiny volumes of carrier gas. Optimal flow rates of 0.02mL/min (future) and 0.2mL/min (current) for N_2 are equivalent to 0.08 to 0.8 mL/min of H_2, based on GC modeling. Electrolytic decomposition of 1 cm^3 of water generates 1300 cm^3 of H_2 gas at 1atm which will last 1 to 10 days at the stated flow rates. The power demand of this electrolysis is 2V * (0.8mL/min) * (1/60 min/s) * ($6*10^{23}$ molecule/mol) * (2 e^-/molecule) / (24400 mL/mol) / ($1.67*10^{19}$ (e^-/s)/amp) = 79mW. Future gas demand of 0.08mL/min will require 8mW and can provide 1-10 days on only 0.1 cm^3 of water.

E: DoD Applications Enabled by Micro GC Based Analyzers

- Remote detection with point sensors
  - Projectile deployed (shoot to where want to sense)
  - Micro aerial vehicle sensors (10-20 mg payloads)
  - Drop deployment (many sensors over area)
- Covert detection capabilities
- Perimeter/facility/building
  - Ventilation sensors for buildings/vessels
- Ring perimeter with sensors
- Improved point sensors for current applications
  - Lighter, faster, more sensitive, more versatile JCAD

References

1. M. L. Hudson, R. Kottenstette, C. M. Matzke, G. C. Frye-Mason, K. A. Shollenberger, D. R. Adkins, and C. C. Wong, "Design, Testing, and Simulation of Microscale Gas Chromatography Columns," Proc. 1998 Int. Mech. Eng. Congress and Expo., Nov. 1998.
2. L. Hancock. "Detection of Nerve Agents Using Fluorescent Reporters," Invited Presentation at Gordon Research Conference on Chemical and Biological Terrorism Defense, March 23-28, 2003.
3. S-W. Zhang, and T. Swager. "Fluorescent Detection of Chemical Warfare Agents: Functional Group Specific Ratiometric Chemosensors," J. Am. Chem. Soc., 125(12), p. 3420-3421.
4. D. S. Ballantine, Jr., S. J. Martin, H. Wohltjen, R. M. White, A. J. Ricco, G. C. Frye, and E. T. Zellers, Acoustic Wave Sensors: Theory, Design, and Physico-Chemical Interactions, Academic Press, 1996.
5. U. Bonne and N. Wong, Private Communication, Aug. 2003; The probability of 1/288,000 corresponds to having only one false positive in one day with a set of 10 detectors that make an analysis every 3 seconds.
6. R. Kottenstette, P. Lewis, D. R. Adkins, G. R. Dulleck, Jr., G. Foltz, S. Gordon, and M. Oborny, "Deployment of a Continuously Operated μChemLab™," Sandia National Laboratories Report SAND2003-1667, May 2003.

3. Parametric Analysis of MGC Column Performance
by Richard Sacks, U. of Michigan , 22 August 2003, rev. 19 Nov. 2003

To determine the capabailities and limitations of μGC with extremely small column diameters, we report here on the results obtained with our GC modeling and optimization programs. We have considered operation of μGC with both pressurized inlets and vacuum outlets, using hydrogen carrier gas.

For the vacuum outlet data, atmospheric inlet pressure was assumed. For the positive pressure data, atmospheric outlet pressure was assumed.
Figures 1 and 2 show the results of optimal column length, max. peak capacity and maximum k-value vs. column diameter, for both 1- and 3-second analyses.

Figs. 3-6 present more recent results for fixed 25 and 50 μm ID columns versus the elution time (up to 0.5 s) and of the last component (analysis time) for both pressurized input and vacuum outlet.
For all plots, the following assumptions were made. We were pleased at the peak capacity values for these extremely fast separations. From the figures, it appears that a peak capacity in the range 5-10 can be achieved for a 25 ms separation. If this is combined with a first-dimension separation producing a peak capacity of say 30 peaks, the 2D separation could have a peaks capacity in the range 150-300 peaks. this would be a remarkable achievement.

- Thin film columns were assumed; thus, band broadening in the stationary phase has been neglected.
- Extra-column band broadening has been neglected.
- Binary diffusion coefficients in hydrogen were assumed to be 0.40 cm2/s
- Binary diffusion coefficients in air were assumed to be 0.08 cm2/s
- Retention-factor value for calculations of plate height was assumed to be 2.0. While plate height does vary with retention factor, assuming a constant value is a reasonable first approximation.

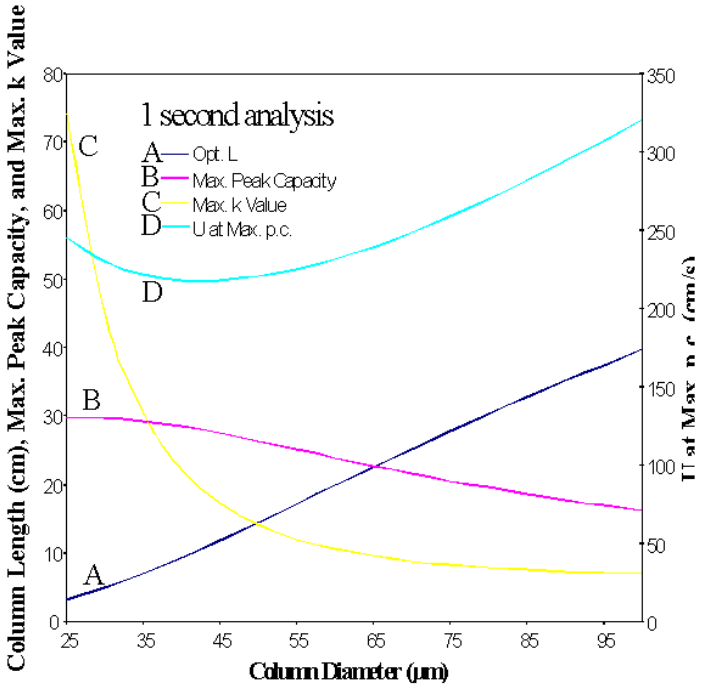

Fig. 1. Vacuum Outlet with Air Carrier Gas

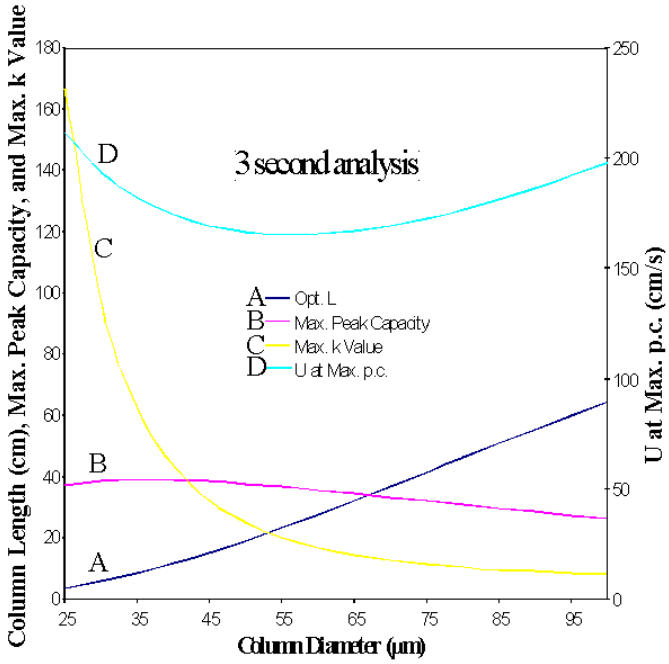

Fig.2. Vacuum Outlet with Air Carrier Gas

The following studies came to mind for future µGC R&D

1. Validate modeling with 0.1 and 0.05-mm i.d. commercial fused silica columns.
2. Model the effects of injection-plug width and detector dead volume on GC resolving power.
3. Investigate fast temperature programming for 3-s separations.
4. Study various stationary phases with regard to stability at elevated temperatures with both wet and dry air as carrier gas.
5. Study mixtures of stationary phases with regard to selectivity for target compounds.
6. Investigate series-coupled column approaches for on-column cleanup to removing interferences prior to detection. (see presentation view graphs for DMMP)
7. Investigate possibilities for two-dimensional GC on a time scale of a few seconds

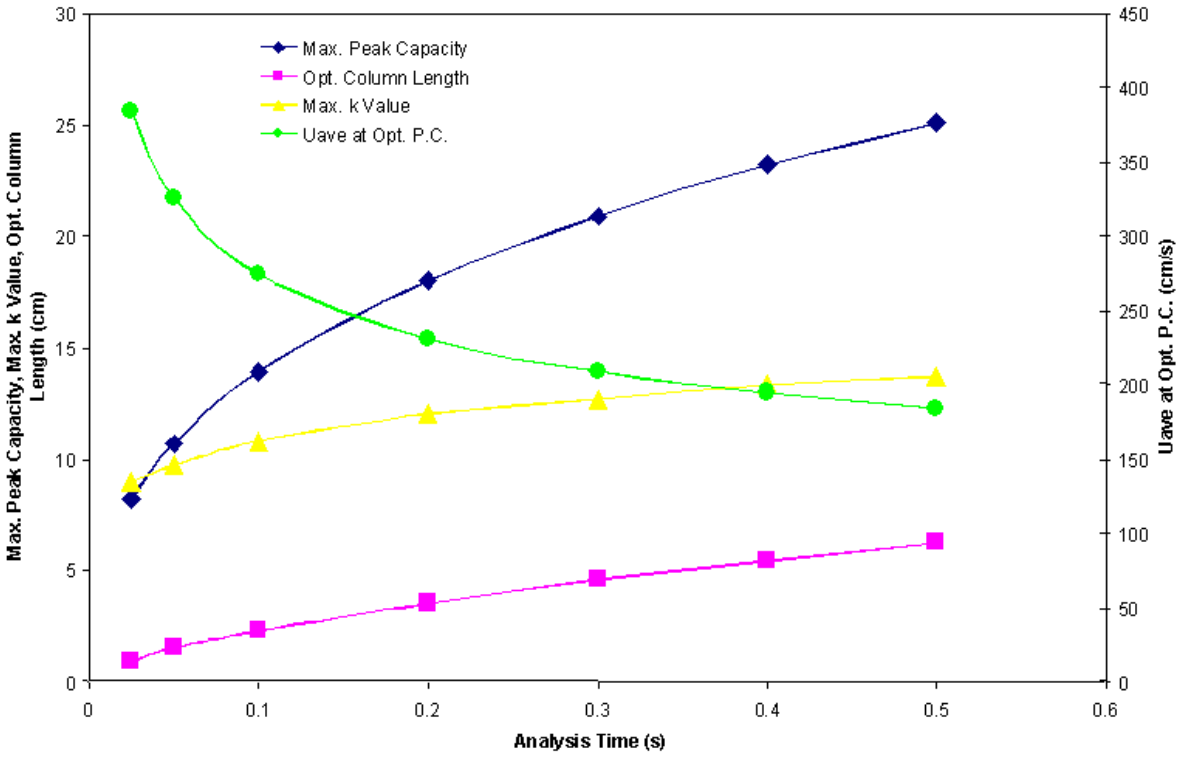

Fig. 3. Positive Pressure Air with a 25 µm ID Column

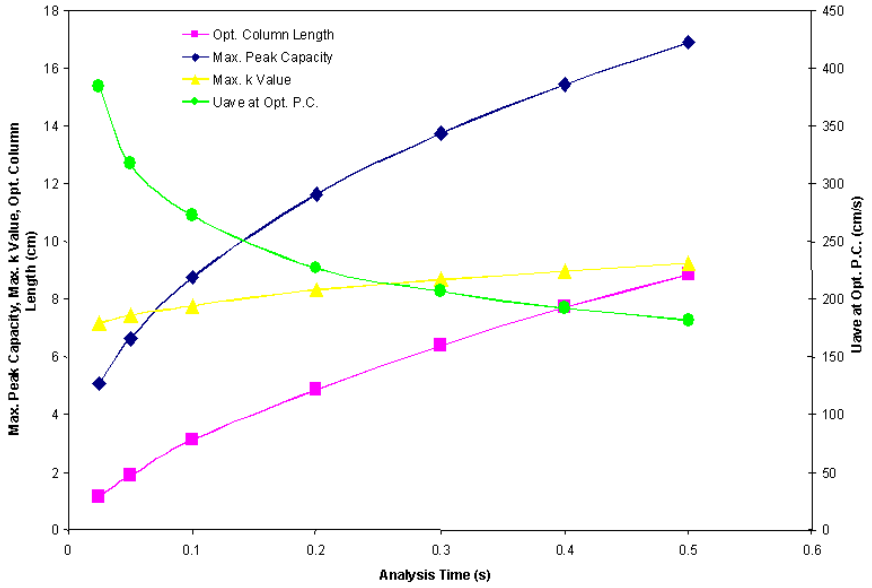

Fig. 4. Positive Pressure Air with a 50 µm i.d. Column

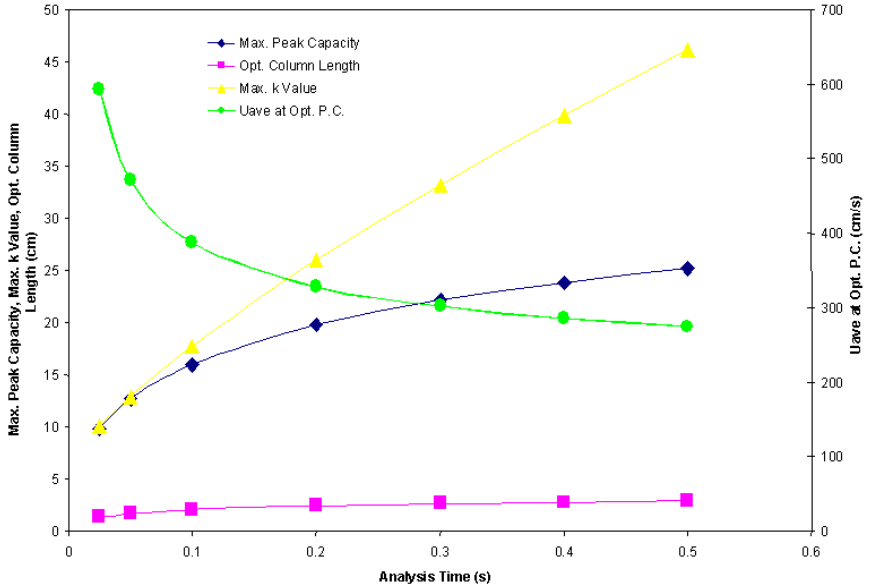

Fig. 5. Vacuum Outlet Air with a 25 µm ID Column

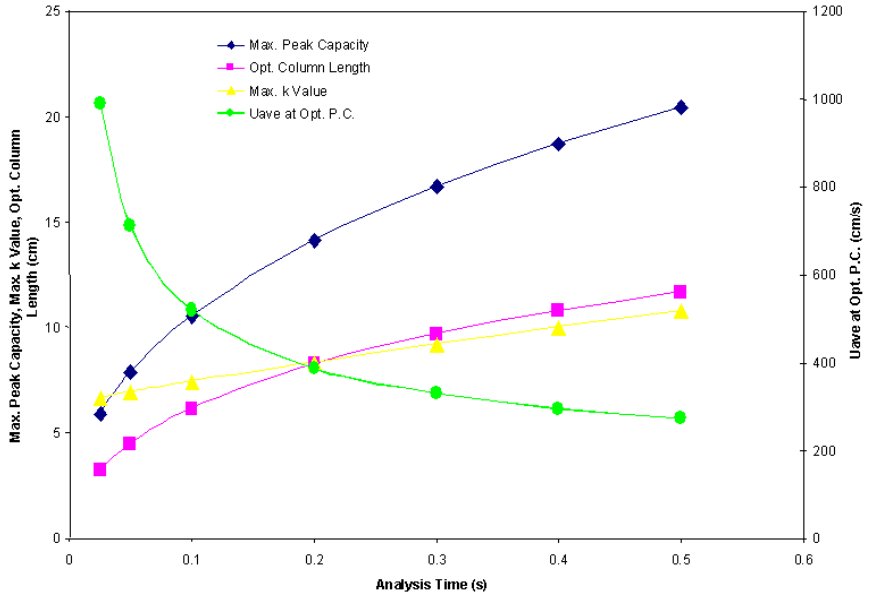

Fig. 6. Vacuum Outlet Air with a 50 µm ID Column

4. High-Speed Micro-GC Performance and Chemometrics, 27 October 2003

Robert E. Synovec, CPAC, Dept. of Chemistry, U. Washington

Overview

Following from the preliminary report (August 2003), the primary focus has been evaluating the potential of high-speed, microfabricated GC. We have focused on several important questions and issues for this study. What are the performance limitations that one can expect for high-speed GC? What is high-speed GC capable of doing and what can be done to improve the performance? What level of peak capacity can be achieved for a 4 second separation? Key to these inquiries is the stationary phase film chemistry. Limitations in stationary phase film technology need to be overcome in order to achieve optimal separation efficiency, N, for a microfabricated GC. What are some reasonable avenues to explore in novel film design and implementation? Finally, what benefit can chemometrics provide for further increasing the effective peak capacity for high-speed GC?

Ideas, calculations and discussion

An overview of high-speed GC performance expectations is provided here, with portions repeated from the preliminary report for continuity and clarity. *Please note, figures cited in the following text are assembled following the text and reference sections.* Given the Golay equation for H, one can plug into equations 1 and 2 in order to calculate the peak width in units of time as observed at the end of the column (i.e., at the detector if no additional band broadening occurs except for the separation process):

$$H = \frac{2D_m}{u} + \frac{1+6k'+11k'^2}{96(1+k')^2}\frac{d_c^{\,2}u}{D_m} + \frac{2k'}{3(1+k')^2}\frac{d_f^{\,2}u}{D_s}$$

$$\sigma_t^2 = (H/L)(1 + k')^2 t_o^2 = ((HL)/u^2)(1 + k')^2 \qquad (1)$$

where the width at the peak base is

$$W_t = 4\sigma_t \qquad (2)$$

with L =column length, t_o = dead time, u = net linear flow velocity, and σ_t = standard deviation of the peak width (Gaussian peak model assumed for simplicity). While H describes the peak width on the column, equations 1 and 2 allow the calculation of the peak width at the detector.

Investigating the possible peak capacity in a four second separation, we began with a list of typical parameters (provided earlier in the EXCEL spreadsheet TL-03-GC-Tradeoff.xls): 100 micron id column, 0.6 micron st. phase film thickness, 30 cm length, gas diff. coef. = 0.15 cm^2/s, u = 100 cm/s, analyte diff. coef. in st. phase = 0.00015

cm^2/s. It is of interest to calculate directly the peak width at the base at various k' using equations 1 and 2. Doing this calculation, H = 0.0062 cm for k' = 0.8 and the peak width at the base, W_t, is 32 milliseconds (ms). According to the Golay equation the contribution to H from the slow mass transfer in the stationary phase is about 10-fold less than the two mobile phase based contributions to band broadening. Thus, stationary phase broadening is not significant even for the relatively thick 0.6 micron phase. The peak width at the base at k' = 7 (near a 3 second retention time as specified at the linear flow velocity given) is 170 ms. Thus, a reasonable peak width average, neglecting the use of temperature programming is to expect peaks ~ 100 ms wide. Now, it is of interest to calculate the peak capacity, n_C, that one would obtain in a 4 second separation, i.e., the number of peaks ideally separated at a specified resolution, R_s,

$$n_C = t_{r,max} / (W_t R_s) \qquad (3)$$

Here, $t_{r,max}$ is the maximum retention time minus the separation dead time, i.e., the useful separation run time, and resolution is defined in the traditional way as

$$R_s = (t_{r,2} - t_{r,1})/W_t \qquad (4)$$

where W_t is now more generalized from equation 2 as the average peak width, in time, at the base for two adjacent peaks with retention times $t_{r,2}$ and $t_{r,1}$, respectively. We note also that resolution can readily be related to the separation efficiency, N, since

$$N = 16 (t_r/W_t)^2 = 5.545 (t_r/W_{1/2})^2 \qquad (5)$$

where $W_{1/2}$ is the average peak width at half height. As N is improved (increases due to instrumentation optimization), the available peak capacity n_C will increase. Now, back to the calculation example using equations 3 and 4, since the dead time is 300 ms for 30 cm length and 100 cm/s linear flow velocity, the 100 ms peak width on average will produce a peak capacity equal to 37 for a 4 second separation at a resolution of one (R_s = 1 constraint). With temperature programming one can expect the peak width to remain ~ 30 ms throughout the run, so a peak capacity of 120 for a 4 second run! (Actually, an even higher peak capacity would be expected since all peaks could ideally elute under k' = 0 conditions, yielding an ideal peak width at the base of 12 ms!)

Going to a 50 micron id capillary and doubling the linear flow velocity in order to keep the mobile phase-related longitudinal and radial mass transfer band broadening contributions equal leads to even better "ideal" separations: W_t = 5 ms at k' = 0, W_t = 11 ms at k' = 0.8, etc. This demonstrates that theoretically with temperature programming a peak capacity of 400 could be achieved in less than four seconds.

So, why is this excellent "ideal" performance (i.e., limited only by the Golay equation) not readily accessible? The limitation appears to be the implementation of dependable injection technology that does not contribute significantly to the band broadening.[1,2] Indeed, we have found that high-speed diaphragm valve injection has provided separations that are on the right track (based on our published work)[3,4] since we routinely achieve injection time constants ~15 ms, yielding a peak capacity of 15 peaks in 1 second. This is an area of research that needs to be explored (we are doing

so now), and the fruits of effectively addressing this limitation should be significant for application of high-speed micro-GC. Thermal-based injection approaches should also be promising if the thermal mass can be minimized and if novel design/implementation approaches can be explored. Using novel injection technology, we have very recently obtained excellent high-speed GC separations, with the unretained peak having a width-at-half-height of 3 ms as shown in Figure 1. The analytes separated in the figure are in the following order of elution: methanol, benzene, octane, chlorobenzene, anisole, decane and butylbenzene. The data presented demonstrate a minimum peak width (at base) of ~ 5 msec, at k' = 0, and ~20 msec at k' = 1 for the isothermal run, following the Golay equation performance. Using temperature programming it is envisaged that peak widths can all be ~ 10 msec, so a peak capacity approaching 100 in 1 second at a resolution of one. Thus, Figure 1 demonstrates that we have refined high-speed GC performance to obtain very minimal band broadening. Indeed, it appears the use of GC to meet the project goals is indeed very feasible.

A key limitation in achieving the desired separation efficiency, N, and thus, the desired peak capacity in a 4 second separation is the performance of the stationary phase in a microfabricated channel structure. Micro GC's based upon microfabrication, due to a square/rectangular channel design, generally suffer from poor N due to poor stationary phase performance. Often the problem stems from the heterogeneous distribution of the stationary phase (generally a polymer) within the channel. Essentially, there is a significant difficulty in uniformly coating the channel with the stationary phase for open tubular GC separations. The non-uniform stationary phase thickness, i.e., too thick in the corners, causes severe peak broadening, essentially a "multi-path" band broadening term not present in the Golay equation. Solving this stationary phase problem is key to achieving the "ideal" peak broadening capabilities. Novel stationary phases will no doubt be part of the answer.

In response to the need for novel stationary phases, we have been developing, in collaboration with Dr. Jay Grate of PNNL, Au-centered monolayer protected nanoparticles (MPNs). These materials appear to have very useful thermodynamic properties (tune selectivity of separation), useful mass transfer properties (fast and effective), and useful thin film characteristics in order to provide state-of-the-art separation efficiency in microfabricated GC devices. Specifically we have been working to characterize the thermodynamic and mass transfer properties of monolayer protected gold nanoparticles (MPNs) using GC, for GC and other sensor applications. Recently, we reported the use of the MPNs as a stationary phase for GC.[5,6] The monolayer applied was a dodecanethiol, providing a separation with chemical selectivity similar to a typical non-polar polymer (see Figures 2 and 3). Figure 2 shows the structure of the particles being studied and Figure 3 shows that the particle diameter is ~ 3 nm. The MPNs appear to have useful properties in that they can be uniformly distributed in a thin film, providing very efficient separations. Indeed, very recently we have shown the MPNs have excellent properties for square channeled capillaries (Figures 4-7), thus the potential appears to be ideal for an efficient microfabricated GC, much better than is available today on the market.[6] Figure 6 is a 2 second GC chromatogram of 7 test compounds using the 100 micron square capillary column (see Figure 4) with the dodecanethiol MPN stationary phase. The elution order of the peaks is methyl ethyl ketone, benzene, octane, chlorobenzene, anisole, 3-octanone and decane.

Novel stationary phases such as MPNs warrant further investigation in order to achieve the goals of the project. Also, use of two-dimensional GC (either GC-GC or GC x GC) should be implemented in order to achieve the desired selectivity to separate the CWAs from background interferences (Figure 8).[3,4] The GC x GC separation in Figure 8 demonstrates that using the proper two stationary phases in concert can provide rapid sample"clean-up" followed by rapid separation of CWA-related compounds. Here, the first dimension is a non-polar stationary phase, separating by boiling point and the second dimension separation is provided by a stationary phase that provides more selectivity toward analyte polarity. In the micro-GC project, one would use a much more rapid "first dimension" for on-line sample prep.

Even with the best available peak capacity, one will want to always push the envelope of applicability, seeking to analyze more complex samples. To address this issue, let's consider the need to implement chemometrics in the data analysis strategy. From our previous work, we have found that the constraint of requiring $R_s = 1$ for the purpose of judging the usefulness of a separation is an artificially determined constraint, born from the days when chromatographers needed to see peaks separated in order to feel satisfied with the methodology. Now with the routine use of computing technology, chemometrics can be readily applied to chromatographic data. Chemometric algorithms do not care if the peaks are separated or not. The key to successful application of chemometric algorithms for chromatographic data is to minimize run-to-run variation in retention time. If retention time variation is minimized, either experimentally or by a robust alignment algorithm, then even a significant degree of peak overlap will not hamper a chemometric analysis of chromatographic data. We have studied this issue extensively for LC[7] and high-speed GC[8] and have found that even down to $R_s = 0.3$ that chemometrics can provide an accurate and precise analysis. Recent data for high-speed GC[8] in Figures 9 and 10 demonstrates that as column length is reduced, absolute run-to-run retention variation is reduced, thus chemometric analysis of this data would be successful even at reduce peak resolution. Using novel retention time alignment algorithms that we have been developing and reported recently, this resolution limit has been pushed even lower.[9] Depending upon the type of chemometric analysis (CLS, PLS, PCA, etc), one can achieve a ~ 3-fold to 10-fold enhancement in the effective peak capacity for high-speed GC separations. For example, using a "GC sensor" with PLS provides excellent data analysis capability in only a 1 second time frame for complex mixtures containing four different classes of compounds.[10] It is not only about separating peaks, but also about providing chromatographic data in a timely fashion that can be readily converted to useful information. Complete resolution is not needed to do so. For the 50-micron id capillary example, this enhancement in effective peak capacity would suggest an effective peak capacity of ~150 to 500 in a half second separation is conceivable, if the injection technology is improved as suggested. In a 4 second separation the information content is proportionately higher.

Conclusions

It seems quite reasonable to achieve substantially higher peak capacities in 4 seconds than has been currently reported by most researchers. Currently, we can baseline separate 7 components in 300 milliseconds (Figure 1), corresponding to a peak capacity of ~ 40 ($R_s = 1$ constraint) for a 1 second separation. This outstanding peak

capacity is achieved by optimizing the injection pulse width, and additional work should be supported to address this need. For a microfabricated GC, novel stationary phases need to be explored in order to achieve optimal separation performance, since typical stationary phases have not performed adequately for microfabricated GC devices. The work with the nanoparticle stationary phases (Figures 2-7) is aimed at addressing this need. Using a combination of GC films with two-dimensional GC approaches will be essential to selectively separate the CWAs of interest from the background (Figure 8). Using chemometrics can significantly enhance the effective peak capacity, and the information content in high-speed GC data can be more readily extracted using a variety of chemometric approaches (Figures 9 and 10). Chemometric methods, and how they relate to high-speed GC use, needs to be included in all modeling and application strategies.

Acknowledgments

I would like to acknowledge the contributions for this study from Dr. Bryan J. Prazen (UW), Dr. Jay W. Grate (PNNL) and Gwen M. Gross (UW, graduate student). Dr. Bryan Prazen and Gwen Gross were integral participants in several of the important pilot studies, results of which are in this report. Dr. Jay Grate is my collaborator on the nanoparticle film technology research.

Literature Cited

1. C.A. Cramers, *Proc. 19th Int. Symp. Cap. Chromatogr. Electrophor.* 1997, p. 2.

2. A. van Es, J. Janssen, C. Cramers, *J. HRC* 1988, **11**, 201.

3. C. A. Bruckner, B. J. Prazen, R. E. Synovec, *Anal. Chem.* 1998, **70**, 2796.

4. K. J. Johnson, B. J. Prazen, R. K. Olund, R. E. Synovec, *J. Sep. Sci.* 2002, **25**, 297.

5. G.M. Gross, D.A. Nelson, J.W. Grate, R.E. Synovec, *Anal. Chem.* 2003, **75**, 4558.

6. G. M. Gross, J. W. Grate, R. E. Synovec, *J. Chromatogr. A*, 2003, submitted.

7. T.J. Bahowick, R.E. Synovec, *Anal. Chem.* 1995, **34**, 631.

8. B.J. Prazen, R.E. Synovec, unpublished work, micro-GC trade-off study, 8/03.

9. K. J. Johnson, B. W. Wright, K. H. Jarman, R.E. Synovec, *J. Chromatogr. A.* 2003, **996**, 141.

10. J. L. Hope, K. J. Johnson, M. A. Calvelti, B. J. Prazen, J. W. Grate, R. E. Synovec, *Anal. Chim Acta*, 2003, **490**, 223.

Figures for High-Speed Micro-GC Performance and Chemometrics

Robert E. Synovec, CPAC, Dept. of Chemistry, U. Washington

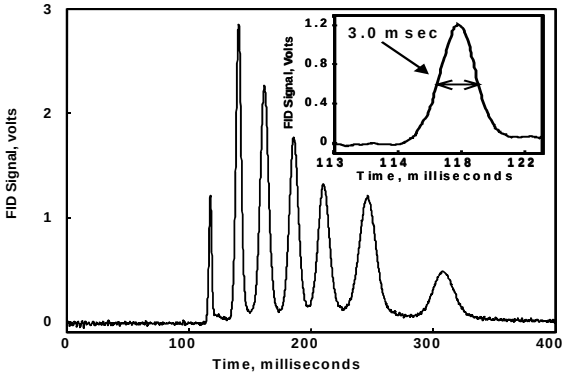

Figure 1. Recent High-Speed GC results (note high efficiency, N). Column: ~ 1 m, 100 micron ID, 0.4 micron film thickness, DB-5 stationary phase.

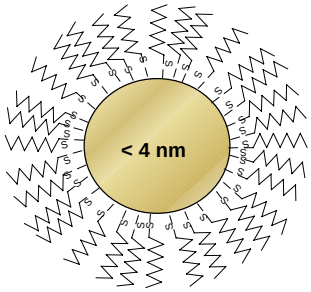

Figure 2. Diagram of monolayer protected gold particle with dodecanethiol surface chemistry.

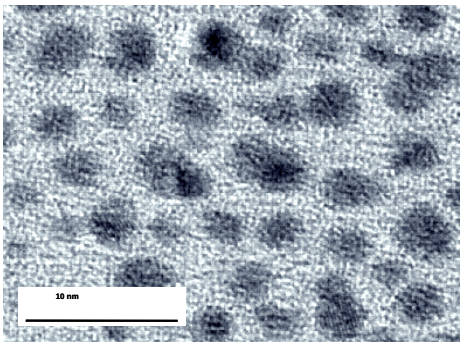

Figure 3 TEM of typical dodecanethiol monolayer protected gold nanoparticles. Bar length is 10 nm.

A)

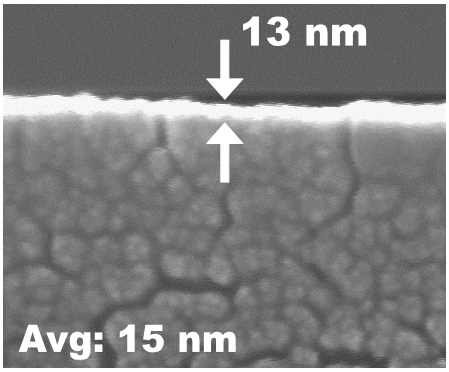

B)

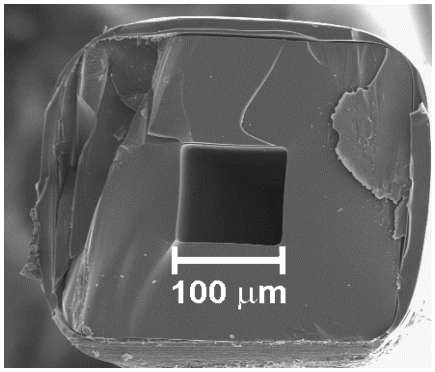

Figure 4. A) SEM image showing the capillary stationary film thickness of square capillaries coated with dodecanethiol monolayer protected gold nanoparticles. The particles had a diameter of approximately 3 nm. B) End-on view of the open tubular square GC column with dodecanethiol monolayer protected gold nanoparticles stationary phase.

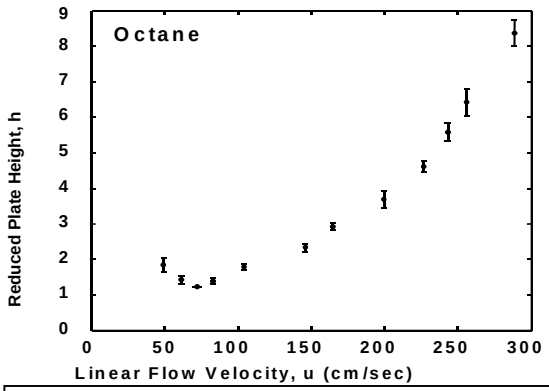

Figure 5. Band broadening performance of square capillary MPN column, k' = 0.3 (octane). An h(min) of 1 is ~ ideal, optimum, following the Golay equation.

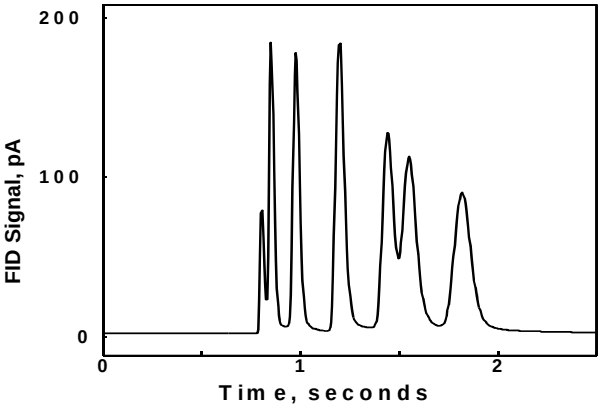

Figure 6. Chromatogram using the square capillary dodecanethiol MPN column.

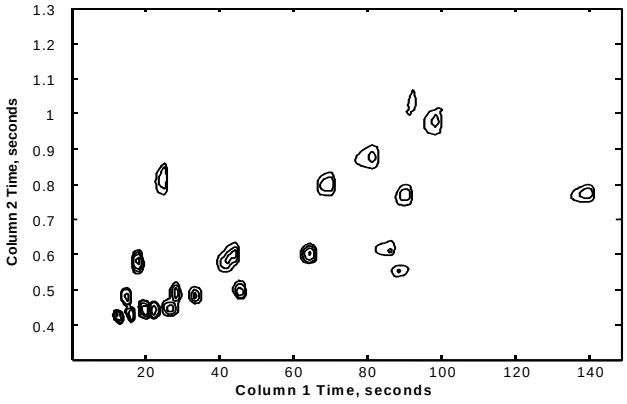

Figure 7. GC x GC using MPN Column (square) in second dimension.

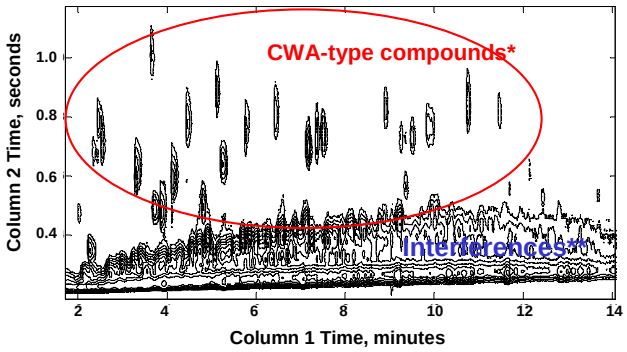

Figure 8. GC x GC of CWA-type compounds in Jet Fuel Sample.

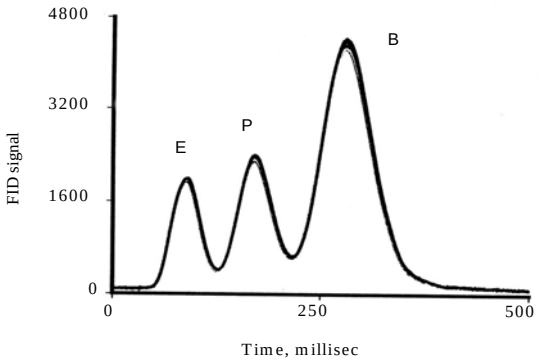

Figure 9. Overlay of 20 injections of Ethanol, n-Propanol and n-Butanol used to Study retention time precision of high-speed GC data.

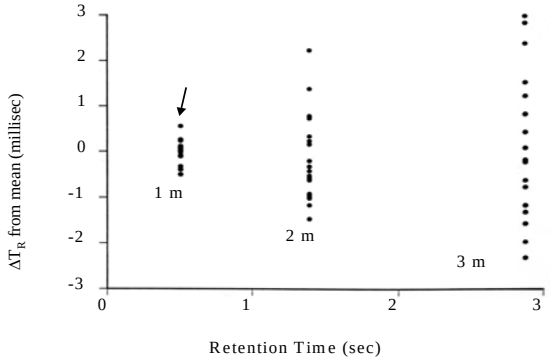

Figure 10. Retention Time Precision for Butanol on 1 m, 2 m and 3 m 250 micron GC columns, same head pressure (8psi).

5. Derivation of a False Positives Model for MGA Comparisons
by Ulrich Bonne, Honeywell Labs, 22 August 2003, rev. 14 Nov. 2003

Driven by the need to minimize false positives in future MGAs[1,2,3], we describe here an attempt to estimate the relative probability of the occurrence of false-positives, P_{fp}, (i.e. reporting the presence of a target analyte despite its **absence** from the sample), or false-negatives , P_{fn}, (i.e. not reporting the presence of a target analyte despite its **presence** in the sample). We will assume that $P_{fp} = P_{fn}$, for purposes of this discussion, which might correspond to a test setup in which target analytes are actually present 50% of the time.

One might expect some relation between a sensor system's S/N ratio, R_{SN}, signal repeatability and cross sensitivity, S_{cross}, and P_{fp}. However, after considering a number of approaches on how to formulate a relation between these, a much simpler concept evolved, i.e. one based on the number of orthogonal or "linearly independent" measurements, n, which the sensor system applies to an unknown sample of one or more known analytes. The larger the value of n, the smaller (and more desirable) P_{fp} would be. Furthermore, to qualitatively assign a relationship between n and P_{fp}, we made the following **assumptions and imposed these constraints**:

- $P_{fp} = f(n^z)$, i.e. that P_{fn}, is some function of n^z, with $0.5 \le z \le 1$
- Trend: $P_{fp} \rightarrow 1$ as $R_{SN} \rightarrow 1$, regardless of the n-value
- Trend: $P_{fp} \rightarrow f(n^z)$ as $R_{SN} \ge 10$, regardless of how much larger the R_{SN} -value might become. In other words, if the signals are stable and well above the noise, further increase of their values does not reduce P_{fp}, because a strong signal only serves to quantify the analytes but not identify them.
- The above R_{SN} only refers to the signal strength. Another signal-to-noise ratio, R_{SNS} refers to the stability of the spectral distribution scale (e.g. uncertainty in the elution time for GC, mass units for MS and wavelength for optical spectrometers), for which similar but separate influences on P_{fp} are expected, but may be lumped in with R_{SN} in this preliminary effort.
- The influence of S_{cross} is included in the value of the orthogonal n measurement elements
- The influence of Repeatability and Drift is included in the value of R_{SN}, as they influence the effective or composite noise amplitude.
- The values of P_{fp} should range from 1 to 0, and therefore $1 / P_{fp}$ should range from 1 to infinity
- The number of analytes, N_g, in the sample gas is fixed (it might be ≤ 20, but is not important here).
- The value of z=1 would correspond to a clean-cut, analytically solvable system as represented by n unknowns and n equations; but a value of n=0.5 would be close to a system in which random statistics dominate. A practical system with quasi-independent elements might perhaps be represented by z=0.8

Upon pondering the analyzer examples described below, we synthesized the following relationships by trial-and-error:

$$1 / P_{fp1} \sim 1 / \{1-(1-1/n)^{0.5}\}, \quad (1)$$

$$1 / P_{fp2} \sim 10\, n^{0.5}, \quad (2)$$

$$1 / P_{fp3} \sim R_{SN}\, n^{0.5}, \quad (3)$$

$$1 / P_{fp4} \sim 1 / [(1 - \exp\{ -(R_{SN} - 1) / 4\}) (n_1 n_2 \cdots n_m)^{0.8} + 1], \quad (4)$$

in attempts to satisfy the above constraints and assumptions. The examples which helped to synthesize the above relations were the first two of those listed below. The others served later as a form of sanity check. Table 1 below lists some exemplary values of the 1/ P_{fpi}, for R_{SN} =1 (rows 1-8) and R_{SN} =10 (rows ≥ 9). The conclusion was that eq.(4) meets the above requirements and constraints. As rationalized above, we used z=0.8. The influence of R_{SN} on P_{fp} according to eq.(4) was plotted in Fig.1. Its caption shows additions to eq.(4) that help to moderate the ability to achieve good P_{fp} values despite low S/N ratios for N >1000. Qualitatively, this may be seen as the benefit of redundancy in overcoming low signal situations. For the analyzer examples derived and described below, we also list the P_{fp} values obtained via eq.(4), first in **Table 1**, and with subsequent updates in the estimated n-values for different detectors as well as ROC curve area values, in **Table 2**.

Table 1. Developmental Calculations of "False Positives" According to Equations (1)-(4)

		1 / Pfp				
RSN	n	z=0.5 Eq.(1)	z=0.5 Eq.(2)	z=0.5 Eq.(3)	z=0.8 Eq.(4)	z=0 Eq.(4)
1	1	1	10	1.0	1.0	
1	5	9	22	2.2	1.0	
1	6	11	24	2.4	1.0	
1	100	199	100	10.0	1.0	
1	200	399	141	14.1	1.0	
1	400	799	200	20.0	1.0	
1	1000	1999	316	31.6	1.0	
1	16000	31999	1265	126.5	1.0	
10	1			10.0	1.9	
10	5			22.4	4.2	
10	6			24.5	4.8	
10	100			100.0	36.6	
10	200			141.4	63.0	
10	400			200.0	109.0	
10	**1000**			316.2	**225.7**	
10	16000			1264.9	2066.0	
10	1000000			10000.0	56446.5	
1	16000			126.5	1.0	1.00
2	16000			253.0	511.6	1.22
4	16000			506.0	1218.9	1.52
6	16000			758.9	1648.0	1.71
10	16000			1264.9	2066.0	1.89
20	16000			2529.8	2289.3	1.99
100	16000			12649.1	2309.3	2.00

- **Array of different polymer sensors**: By coating every sensing element of an array with n different or differently doped polymer (or metal oxide) films, one could envision that: the quantity of an analyte can be sensed by the observed **signal size** and the identity of the analyte by the **pattern** (or spectrum) of signals. The probability of making an error in compound identification would therefore be equivalent to the probability of false positives (P_{fp}) or false negatives. In practice, this approach has shown to not add new (i.e. independent) information beyond an equivalent of ~5-6 truly independent sensor materials and signals. In other words, even massive arrays of such sensor elements are no more selective than sensors with n ≥ 5-6[4,5]. For such values of n and assuming large values of R_{SN} = 10, we get P_{fp4} = 1:4.2 to 1:**4.8**. The blue value for n was included in the summary **Table 2**. The corresponding ROC curve is shown in **Fig.2**.

- **NDIR spectral correlation**: Same as above with many more array elements (=wavelength bins), with less relative drift, but a requirement that each bin corresponds to individual, spectrally resolved (i.e. orthogonal!) elements. If not resolved, n would be reduced until this

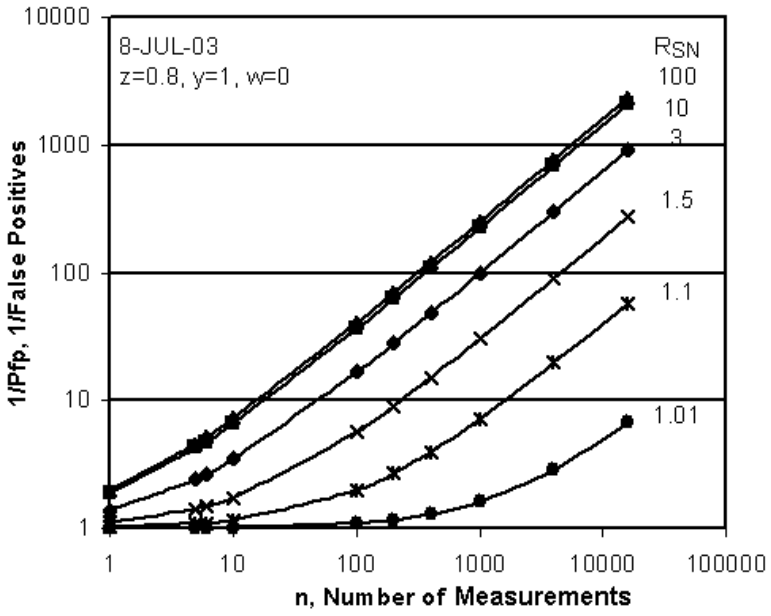

Fig. 1. Inverse of False Positives vs. n and R_{SN} Influence

$$1/P_{fp} = (1-\exp(-(R_{SN}-1)/4)^{(y/n^w)})\, n^z + 1$$

condition is met. For n=**100** to 1000, we get P_{fp4} = 1:**37** to 1:226. The smaller number applies especially to small, portable devices, such as the Polychromator(6).

- **GC with non-selective detector (TCD or FID):** Now we only have the resolvable elution time elements to form an array. They might range from 100 to1000 for a short 50-cm capillary-column μGC to a SOA 50-m-GC column. The TCD does not add any orthogonality and therefore we get P_{fp4} = 1:37 to 1:226. More recently we determined that a "peak capacity" of ~**50** would represent a considerable challenge to MGC, which is why this number is used in Table 2 for a MGC and **200** for a std. GC.

Table 2. Estimated, Relative False Positive Fraction(FPF*) and Area above ROC Curve for Analyzer Examples,

(Test Assumption: Target analytes are actually present 50% of the time, so that TPF ~ TNF; FPF=Pfp)

#	Gas Analyzer Example	Y	n	1/Pfp**	TPF	d'	1-Az(ROC)
1	Array of different polymers, CID (e.g. nanocant.),	1	**5.5**	5	0.800000	1.6832	**1.17E-01**
2	MGC with non-selective detector (TCD or FID)	1	**50**	22	0.954545	3.3812	**8.40E-03**
3	NDIR spectral correlation (e.g. Polychromator),	1	**100**	37	0.972973	3.8528	**3.22E-03**
4	Std.GC with non-selective detector (TCD or FID)	1	**200**	63	0.984127	4.2952	**1.19E-03**
5	MGC with one multi-channel det. (MDOD), 50 x 10	1	**500**	130	0.992308	4.8464	**3.05E-04**
6	MGC with 2 multi-channel det. (MDOD and FD), 50x10x4	1	**2,000**	392	0.997451	5.6015	**3.74E-05**
7	MGC-MGC-MDOD combination, 50 x 10 x 10,	1	**5,000**	815	0.998774	6.0583	**9.19E-06**
8	Std.GC with 2 multi-channel det. (MDOD and FD), 200x40	1	**8,000**	1,187	0.999158	6.2818	**4.46E-06**
9	MGC-MS combination, 50 x 300	1	**15,000**	1,962	0.999490	6.5705	**1.69E-06**
10	Std.GC-MS "Gold Std." combination, 200 x 300	1	**60,000**	5,946	0.999832	7.1712	**1.98E-07**
11	MGC-MGC-CID-PID-MDID-MDOD, 50 x 10 x 6 x 4 x 10	1	**120,000**	10,352	0.999903	7.4552	**6.77E-08**
12	MGC-MGC-CID-MDID-ITMS, 50 x 6 x 2 x 300,	1	**180,000**	14,318	0.999930	7.6182	**3.59E-08**
13	MGC-MGC-CID-MDID-ITMS, 50 x 6 x 2 x 300,	100	**180,000**	18,000,000	1.000000	~11.7	**~3.0 E-14**
14	MGC-MGC-MDOD combination, 50 x 10 x 10,	100	**5,000****	500,000	0.999998	9.2387	**3.24E-11**

* $1/P_{fp} \sim [1 - \exp\{-(RSN - 1)/4\}]^{Y (n1n2....nm)^{0.8} + 1}$

** 1/Pfp = 1/288,000 corresponds to one FP/day for all analyses performed in 1 day every 3 seconds by 10 analyzers

TPF=True positive fraction

FPF = False positive fraction

Az = Area under the ROC curve, TPF vs. FPF

d'=Distance between the mean values of the Noise and Signal+Noise Gaussians

- **MGC with multi-channel detector(s)** (micro-discharge optical detector (MDOD) or/and fluorescence detector (FD)): Now the above n-value of ~50, would get augmented by the number of differentiators we can implement with these detectors. By using just one of the two or both (of these orthogonal detectors) the number of independent measurements would increase by 10x, 4x or 10x4=40x. The totals could then be n = 200, 500 or 2000. Rows 5 and 6 in Table 2 include the latter 2 values, leading to a range of P_{fp4} = 1:**130** to 1:**815**.

- **Combination of Standard GC-MS** - the "Gold Standard"(2) - might result in a system with n = 200 x 300 = **60,000** and P_{fp} = 1/**5,946**, i.e. close to a 100x reduction in P_{fp} relative to a std. GC with an FID, and off the chart in the graphical representation of $P_{fp}(n)$ in Fig.1. Still this system cannot achieve the compactness, low-power and sensitivity goals mentioned earlier. The sensitivity limit may be overcome via addition of suitable multi-stage pre-concentration(8). The area above the ROC curve or system error rate is $\mathbf{2 \cdot 10^{-7}}$ or 1 in 5,000,000

A more recent insight on how to further reduce false positive rates from the present level(7), is by networking a number of characterized (not necessarily equal) detectors. This improvement is reflected in the above model by the addition of the factor, Y, to eq.(4), see bottom of Table 2, that represents the benefit of simultaneous operation of networked sensors. A value of Y~100 might be achieved by

reducing the uncertainty of an analyzer response, with a logical network of e.g. 10 analyzers, thus enabling MGAs of Table 2 to pass the P_{fp} = 1/288,000 milestone[9]. A factor of Y~100 may be achieved by the following combination of factors:

- **2x** if a positive signal or "hit" is accepted and acted upon only if both **redundant analyzers** in close proximity show similar signals, which means that the network has 5 pairs of analyzers at different locations;
- **32x** by keeping track of the location of each analyzer pair (e.g. spaced in a "die-4 or -5 pattern" so that the space s > v t, such that wind of velocity, v, should trigger the alarm level in time increments no smaller than the analyzer update time, and have that be consistent with **wind direction** (8 bins) and **wind speed** (4 bins); and
- **2x** by comparing the signal timing between a **ground- and high-level** sensors (e.g., one analyzer of the middle of the 5-pairs, raised to ~ 10-20 meters), whereby the latter should reach alarm level sooner due its exposure to higher wind velocity

Total factor of false positives reduction might then for this case be, Y = 2 x 32 x 2 = 128.

Table 2 presents an updated summary of the analyzer examples discussed above, with updated n-values relative to those presented earlier[3], the estimated equality FPF=P_{fp} and values of TPF=1-FPF by virtue of the test set up, which provides for target analytes to be actually present 50% of the time, and the computed ROC curve data: d' = distance in std.dev. units between the mean of the assumed normal distribution of noise and the mean of the signal+noise; and 1-Az, i.e. the normalized area above the ROC curve, see Fig.2, which is a measure for the fraction of incorrect analyzer outputs. Among extensive discussions on detector statistics in the literature[10-15] I derived the most useful insights in working with Dale Berger and Mike Healey at Claremont University[15] and especially with M.Healey, who provided the ROC programming expertise and the core of the ROC calculations in Excel, which is enclosed as a new addition to the set of simulation models

Conclusions

1. The false positives model derived to date, despite its infancy state, is helping to provide a generic comparison among alternate detection/analyzer technologies, with respect to their ability to minimize false positives. This generic comparison is one that is based on very idealized or generic test conditions
2. The model was set up to satisfy a set of constraints on the influence of S/N ratio, associated drift, but most importantly, the total number of independent measurements and number of different levels or types of meaurement. The addition of each new and different (i.e. orthogonal) analysis techniques, n_2, n_3, ...n_i, to a first analysis technology, n_1, increases the total "n" as n = $n_1 x n_2 x ... n_i$, and can significantly decrease the number of false positives (and false negatives).
3. Networking and redundant analyzers can provide additional reductions in P_{fp}, which may amount to factors neat 100x for a network of only 10 analyzers.

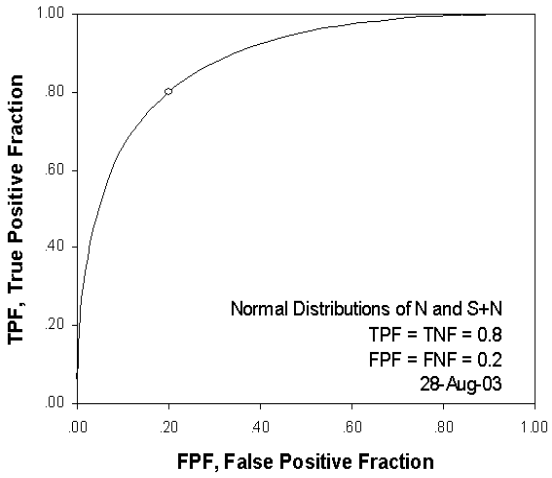

Fig. 2. Receiver Operating Chracteristic (ROC)

References

1. Clark Nguyen and Bill Snowden, DARPA Workshop on Micro Gas Analyzers, Monterey, CA, 16-17 December 2002. Proceedings on CD;
2. Clark Nguyen, "Micro Gas Analyzer," DARPA BAA 03-40, 15 Aug. 2003
3. U.Bonne (Honeywell Labs), G.Eden (U.Illinois), G.Frye-Mason (Nomadics, Inc.), C.Herring (Caviton, Inc.), R.Sacks (U.Michigan) and R.Synovec (U.Washington), "Micro Gas Chromatograph Tradeoff Study - Interim Report," to DARPA-MTO/AFRC/UTC for BAA N66001-03-X-6001, 25 Aug. 2003

4. Greg Frye-Mason, Private Communication (Ted Zeller et al, sensing with array of polymeric film elements showed that for n > 5, analysis results were very unreliable, even with a constrained set of analytes), 1 July 2003
5. Ulrich Bonne, Private Communication, in relation to a Honeywell-GRI Contract ~1980s; in using arrays of SnO2 elements w/different doping the researchers found poor convergence with more than 5 sensors in the array, 1 July 2003
6. G.B. Hocker, D. Youngner, E. Deutsch, A. Volpicelli, S. Senturia, M. Butler, M. Sinclair, T. Plowman and A.J. Ricco, "The Polychromator: A Programmable MEMS Diffraction Grating for Synthetic Spectra, *2000 Solid State Sensor and Actuator Workshop*, Hilton Head, SC, June 5-8, 2000, Technical Digest pp. 89-92
7. Ngai Wong, Private Communication "What is available is the current false alarm rate which is typically 1 alarm in about 150 hours for a single detector," 30 March 2003
8. U.Bonne, J.Detry, R.E.Higashi, T.Rezacheck and S.Swanson, "New Gas Composition and Trace Contaminant Sensors," GTI Gas Technology Conference, Orlando, FL, 30 Sep. - 2 Oct. 2002, Proceedings
9. Ngai Wong, SBCCOM, Private communication, "Achieving a false positives rate of only one per day with a set of 10 detectors of which each provides air analyses every 3 seconds, would be a worthy goal", which corresponds to Pfp < 1/288,888; Aug.'03
10. David M. Haaland; (Sandia Corporation, Albuquerque, NM), "Classical least squares multivariate spectral analysis," U.S.Pat. 6,415,233, 2 July 2002
11. Christina Müller, Martina Scharmach (Federal Institute for Materials Research and Testing (BAM), Germany, Christina.Mueller@bam.de, Martina.Scharmach@bam.de), Vera Konchina (NIIM/PGUPS, St. Petersburg, Russia, konshina@ndtcenter.spb.ru), Damir Markucic (Faculty of Mechanical Engineering & Naval Architecture, University of Zagreb, Croatia, damir.markucic@fsb.hr), Zeljko Piscenec (Croation Mine Action Centre, zeljko.piscenec@hcr.hr), "General Principles of Reliability Assessment of Nondestructive Diagnostic Systems and Its Applicability to the Demining Problem," NDT.net - April 2003, Vol. 8 No.4, http://www.ndt.net/article/ecndt02/397/397.htm Paper presented at the 8th ECNDT, Barcelona, Spain, June 2002
12. Frank Schoonjans, "ROC curve analysis: introduction," Version 7.2.0.2 - Last modified: 24 July 2003 - email: info@medcalc.be, http://www.medcalc.be/manual/mpage06-13a.html
13. Computation of Area under ROC and Gaussian Error Curves http://www.nhn.ou.edu/~marzban/roc.pdf
14. ROC Functions: http://psych-www.colorado.edu/~lharvey/P4165/P4165_2003_Spring/2003_Spring_pdf/P4165_SDT.pdf
15. Dale E. Berger and Michael Healy, Clarement Graduate University, Clarement, CA, Private Communications; http://wise.cgu.edu/sdt/sdt.html computes and displays ROC curves on line. Signal Detection Theory. Gaussian Model; Dale.Berger@cgu.edu, Michael.Healy@cgu.edu

6. Capabilities of Laser-Based (VCSEL or edge-emitting) **Optical Absorption Approaches by Ulrich Bonne, Honeywell Labs, 18 October 2003, rev. 15 Nov. 2003.**

Summary. In exploring what the limits of optical CWA point detection might be and whether they might be amenable to meeting the DARPA MGA goals of 1 ppt, 2 cm^3, 1 J, 4 s and minimum false positives, the 1 ppt and 2 cm^3 stand out as the most challenging ones.
Via the thought process presented below, we conclude that to sense 1 ppt worth of CWAs at their fundamental, mid-IR range, and most optimistic absorption strength, the MGA would need to be able to perform absorption measurements with a S/N ratio of ~ 1/2.5 ppb if using a L=10-cm optical path, and would correspond to a detection limit of 0.000 000 1 ppm-meter. A light trap to increase the optical path in a 1-cm-ID cell 100x to L=1000 and a more realistic absorption strength (10x less) would reduce the detection requirement 10x to ~ 0.000 001 but still be out of reach by ~4-5 orders of magnitude, before meeting the needed D_L~0.01 ppm-meter threshold of achievable optical detection of a strongly absorbing molecule, derived below, see **Table 1.**
By way of reference, 1) A tunable laser opto-acoustic sensing system presented at a DOE Annual Review in June 2003 achieved an MDL of 10 ppb of acetylene near the fundamental absorption of 3 μm in a ~1,000-multiple-internal reflection light trap of 20 cm ID worth 200 m of optical path and thus corresponding to D_L = 2 ppm-meter[1,2], 2) We detected < 1 ppm CO in a 10-cm-single pass cell, via frequency modulation at 4.6 μm, corresponding to D_L = 0.1 ppm-meter[3,4] and 3) The most strongly absorbing gas in the HITRAN data base is SF6 at 10.55 μm, with an absorption coefficient of $a=3455 \cdot 10^{-20}$ cm^2/molecule, or ~15x larger than that of CO, leading to a D_L~0.01 ppm·m.

Standard Absorption Approach. To obtain maximum signal strength, the preferred approach is to sense the gas of interest at its fundamental absorption, which is typically located in the mid-IR for vibration-rotational excitation, in the far IR/microwave for pure rotational excitation and in the vis/UV for electronic excitation. Unfortunately, low-cost and low-power light sources are not readily available at the mid- or far-IR, where all non-symmetric gases have useful absorption bands.

To match gas detection in the 2-6 μm range to the available 0.7 to 1.2-μm near-IR laser outputs, one can consider higher harmonics of the fundamental molecular oscillations. The HITRAN data base[5] shows that absorption at higher harmonics shifts the wavelength closer to low-cost lasers, although this comes at the price of reduced absorption strength, with 1st and 2nd harmonics for example NO near 2.7 and 1.8 μm but a 58x and 3364x reduction in absorptivity. The **Table 1** below summarizes such data for a few gases. The last column cell lengths are based on earlier calculations in which we estimated the cell length needed for a 1 ppm CO sensor, assuming a min. measurable absorption of 1/10,000.[1,2].

The detection limit of this classical NDIR absorption approach, based on fixed-wavelength source and detector, on-off chopping of the transmission, and ability to measure an absorption signal of ~ **1:1,000** (corresponding to a detection limit of **D_L = 300 ppm·m for the CO example**), can be improved as follows:

1. **Narrow Light Source Line Width:** Reducing the half-height-width of the light source, e.g. from 12 nm to 0.4, the CO detection limit with a 10 cm optical cell (one pass) would improve to **D_L = 100 ppm·m,** if laser sources at 4600 nm were available. D_L would deteriorate by >1000x if the 2nd harmonic vibrational transition was to be used to bring the wavelength range closer to the available VCSEL range.
2. **Frequency Modulation:** I.e. modulation of the source wavelength line or band, e.g. via Fabry-Perot interferometry by modulating the source wavelength between on and off-line or -band[2,3]. With laser sources, which provide strong & narrow signals, this measurement method is independent on the laser intensity, provided that it is 10,000x higher than the detector noise threshold. The detection limit of CO might be improved to measure absorption signals as low as **1:10,000**, i.e. A_{max} =

0.0001, which correspond to a limit of **D_L = 0.1 ppm·m for CO,** and was assumed for generating the data in Table 1.

Table 1. On the limits of gas detection via IR absorption, using fundamental, 1st and 2nd harmonic absorption bands

	Abs. Fund.*	Decrease in Abs.		Wavelengths in μm*			Practical Cell	Det.Limit
	cm^2/molec	1st Harm.	2nd Harm	Fundam.	1st	2nd	Length in m**	ppm·m
NO	$80 \cdot 10^{-20}$	58x	3364x	5.30 ± 0.2	2.69	~1.77	0.28 /16/ 930	0.28
NO2	$316 \cdot 10^{-20}$	32x	1000x	6.2 ± 0.1	3.4	~1.9	0.07 /2.2/ 70	0.07
CO2	$1232 \cdot 10^{-20}$				4.3		0.017/ /	0.019
CO	$206 \cdot 10^{-20}$				4.6		0.10 / /	0.1
C2H2	$71 \cdot 10^{-20}$				3.1		0.29	0.29
CWA.	$\sim 1000 \cdot 10^{-20}$				~3.1		0.2	0.02
SO2	$89 \cdot 10^{-20}$	286x	66000x	8.0	4.0	2.5	0.23	0.23
SF6	$3460 \cdot 10^{-20}$			0.55			0.006	0.006
BB	$1{,}000{,}000 \cdot 10^{-20}$ ("black-body" molecule of 10 x 10 Å in cross section)						$2 \cdot 10^{-5}$	$2 \cdot 10^{-5}$

---

* From the HITRAN data base(5);

** Single-pass cell, to sense 1 ppm w/absorption of 1:10,000, at $\Delta\lambda \leq 0.4$ nm. Natural line width at 4600 nm is ~0.2 nm. The listed numbers separated by slashes represent the needed cell lengths (read: optical paths) for the fundamental, 1st harmonic and 2nd harmonic bands

3. **Opto-Acoustic Detection (OAD)**: Back to on-off chopping of the light source, but change the detection scheme from optical absorption to opto-acoustic, -thermal or -flow, which removes the S/N dependence on optical path length and makes it dependent on:
   a) The volumetric ratio of V_S/V_C = (gas volume swept by the source beam)/(volume of the gas cell), whereby the effective source beam volume increases as the number of passes increases, until absorption saturation is approached, if ever. By way of reference, the classical single-pass absorption scheme starts out at $V_S/V_C = 1$
   b) Source intensity. Absence of the analyte of interest theoretically generates zero modulation signal, so that one might expect to achieve a 3-fold improvement and achieve **D_L ~ 0.03 ppm·m for CO**. Higher improvements would theoretically be possible, but are typically thwarted by synchronous scattering noise levels. This still assumes availability of laser sources at the fundamental absorption band
4. **OAD + Frequency Modulation**: Same as #3 but with the addition of modulation of the source wavelength-line (or -band). This should reduce synchronous noise and may improve the detection to **D_L ~ 0.01 ppm·m for CO**, which is what PSI(4) and LGR(5) achieved with a wavelength-modulated, mixed-VSCEL light source near 3100 nm (mixing 1000 nm + 1500 nm VCSELs to generate the beat wavelength of 3000 nm, whereby one VCSEL cavity was modulated via a dithering grating) with a multiple internal reflection cell (20-cm light trap) to sense acetylene down to the ~ 10 ppb level. Note that this corresponds to sensing absorption levels of A_{max} = 0.00001 or 10 ppm of signal, i.e. equivalent to a S/N ratio of 100,000:1.

To translate the above insights into a generic statement on the limitation of optical absorption, we calculated what the maximum ability of a compact optical detection system would have to be, in order to be able to sense 1 ppt of CWA in an optical path of L ≤10 cm. The estimated maximum optical absorption, A_{max}, generated by x = 1 ppt concentration of molecules is related to their optical cross section, a = 100 $Å^2$ per molecule (or $a=10^{-14}$ cm^2/molecule; this assumes that each molecule acts like a small disk of

black body and is >1000x higher than the highest a-values listed in the HITRAN data base). For L = 10 cm path length, ambient pressure (p = 1 atm) and ambient temperature (T = 298 K), the Avogadro number of molecules in one molar volume of V_M = 22415 cm^3 at p_o and T_o translates to:

$$N = 6.02257 \cdot 10^{23} (T_o/T)(p/p_o)/V_M = 2.4614 \cdot 10^{19} \text{ molecules/cm}^3.$$

With $A_{max} = x \cdot a \cdot L \cdot N$, in $cm^2 \cdot cm / cm^3$, we can calculate $A_{max} = 10^{-12} \cdot 100 \cdot 10^{-16} \cdot 10 \cdot 2.4614 \cdot 10^{19} = 2.46 \cdot 10^{-6}$ or **A_{max} = 2.46 ppm**. Considering that the highest absorption coefficient, a, of any line in the HITRAN data base is about 1000 lower ($a \leq 10^{-17}$ cm^2/molecule), we should count on finding that the maximum absorption for analytes of interest will likely be **$A_{max} \leq$ 2.46 ppb of signal** (for x = 1ppt and L = 10cm), i.e. quite out of reach of known composite stability ranges of "light source and detector" systems, despite opto-acoustics and frequency modulation aids discussed above.

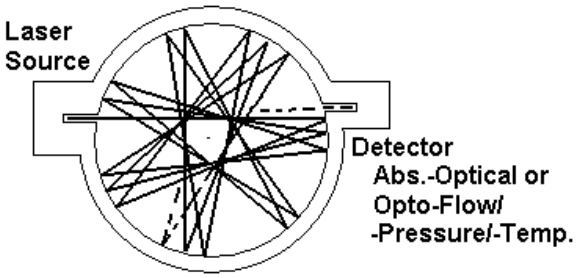

Fig. 1. Inner-Reflective Sample Cell, with Micro-Holes for I/O of Sample and Optical Beam

Opto-Acoustic Detection (OAD) Approach. A sketch of one approach of this type is shown in **Fig.1.** The flat-cylindrical shape of the cell (preferred design w/~100 μm depth to minimize its volume for fast purge, but still enable interface with detector(s), which could be a photo-detector, a microphone and/or a thermal detector) would be highly reflective for the wavelength of interest (e.g. using Au plating for IR wavelengths). The multiple internal reflections would also benefit above Case #1 of std. absorption (long path), but for the OA approach the laser light needs to fill the volume of the whole cell (opto-acoustic sensors are most efficient when the cell volume equals the volume of the laser beam, and the laser intensity causes all available molecules to be excited to the upper energy level).

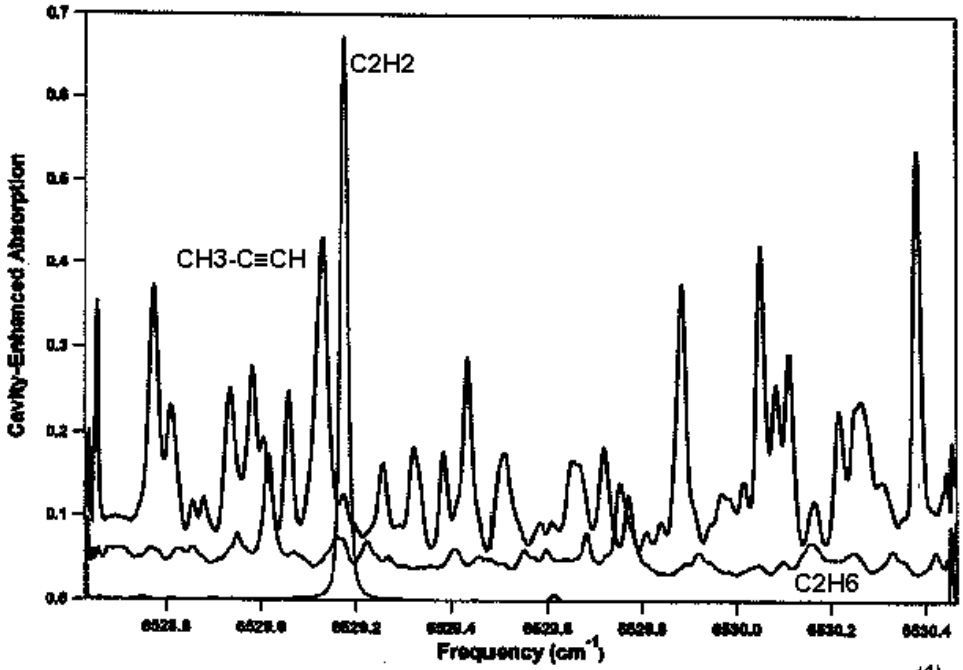

Fig. 2. Measured Spectra of Three Hydrocarbons in the 1500-1600 nm range.[1]

Challenges for both above approaches are caused by natural line width limitations and resulting interferences as exemplified by the high-resolution spectrum in **Fig.2**, showing the targeted absorption lines of only C2H2, H3C-C≡CH and C2H6 in the 1500-1600 nm range, and in **Fig.3** for the fundamental CH-vibration band in the 3154-3424 nm range. Such detection systems have been demonstrated to achieve minimum detection levels of ~ 10 ppb of C2H2 in ethane, with multiple (>10,000 ??) internal reflections in a 20 cm cell[1,2]. This would correspond to a surprisingly poor D_L = 20 ppm·mIn. In comparing these results with those obtained in the lab with CO absorption[3], and in taking into account the ~3x difference in the absorption coefficient, we conclude that maybe the

total number of internal absorptions may have been somewhat lower, possibly in the 300-1000 range, which would better harmonize with other data in Table 1.

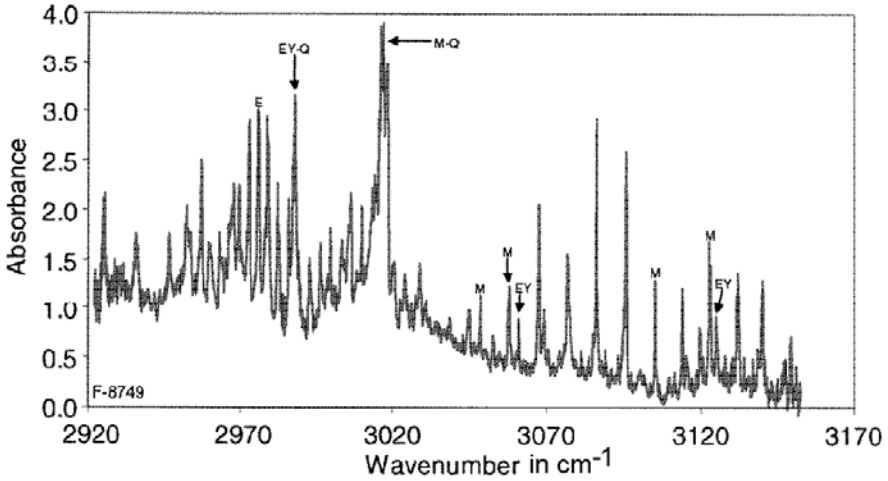

Fig. 3. Absorption Spectrum of a Hydrocarbon Mixture of 2.8% CH4(M), 4.9% C2H6(E) and 9.3% C2H4(EY) in N2 at p=720 Torr, Obtained via 250 cm^{-1}-Range, Tunable Diode Lasers. By D.Bamford et al, PSI(2)

References

1. M.Gupta et al (Los Gatos Research, Mountain View, CA), "Cavity-Enhanced Gas Analyzer for Process Control Applications," DOE-S&A Annual Review, San Francisco, 3-4 June 2003
2. D.Bamford, et al (PSI, San Ramon, CA), "Broadly-Tunable Mid-Infrared Hydrocarbon Sensor," PPT presentation, DOE-S&A Annual Review, San Francisco, 3-4 June 2003
3. J. J. Barrett, “Infrared Gas Analysis” U. S. Patents 3,939,348, 17 Feb 1976, and 4,035,643, 12 July 1977, assigned to Allied Chemical Corporation (now Honeywell)
4. U.Bonne, Internal Honeywell Report, 2001
5. A.Rothman et al, "HITRAN Data Base," Cambridge AFB and Harvard University; updates since 1996

7.0 Evaluation of Ion-Drag and Fluidic Diode Pumping Approaches, 19 Nov. 2003 by U. Bonne, Honeywell Labs

Introduction. Presently available MGA gas sampling pumps for microanalytics are bulky, comprise mechanical actuators that are prone to wear, limit their service life, and create undesirable flow pulsations that need to be dampened via bulky buffer volumes. The cost to fabricate and assemble such mechanical-actuation pumps (regardless of whether they are based on electro-magnetic, piezo-electric or electro-static forces) is high and contributes to their high cost.

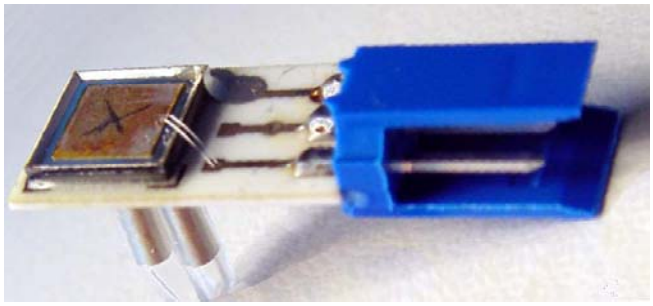

Fig. 1. Piezoelectrically Driven Silicon-Based Micropump, by Fraunhofer Inst.(21).

The pump concepts evaluated below might eliminate above shortcomings by generating a steady gas flow, which is driven by viscous **ion-drag** created by a small volumetric fraction of large (relative to the electrons), in-situ-generated ions, which then drift in response to an applied electric field and drag neutral molecules along[1,2], as Honeywell is using in desk-top electrostatic air cleaners and liquid microanalysis systems have been using for some time. Micro-scaling favors achieving high fields with low voltages and high localized ion concentrations and high localized plasma energy densities[3,4], as discussed in above Section D.1. Additional approaches based on "valveless" pumping in the form of **fluidic diodes** might be used synergistically with the above ion-drag approach, despite the traditional oscillatory membranes used to drive such pumps. Ion-drag- and fluidic-diode-pumps have been developed successfully for pumping of liquids[5,6] but only sporadically for gases[6,7].

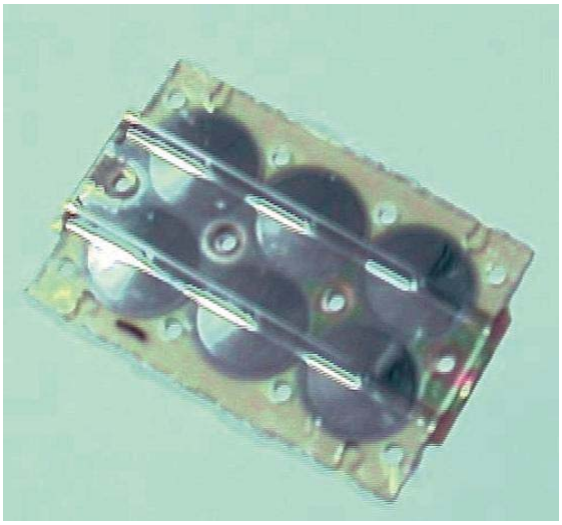

Fig. 2. Photograph of One Layer of Double-Diaphragm, MesoPumps w/~10 mm ID Actuators

The desire to explore and evaluate alternate, non-moving-parts gas pumping does not imply lack of recognition for past successful progress with piezoelectric[8,9] and development of electrostatic approaches[10]. Rather, the potential benefits of increasing pumping energy efficiency from the present ~ 5% level and reducing pump size seem too compelling to pass up.

By way of examples of mechanical pumps, **Fig. 1** shows a micro pump based on piezoelectric actuation([9], with some performance data listed in **Table 1**. The photo in **Fig. 2** shows a cluster of electro-statically actuated MesoPumps developed at the Honeywell Labs[10]. As shown, the power needed to pump an exemplary 1.4 scm^3/min against a head of 9.7 psi (~669 mbar) corresponds to an efficiency of up to ~8% for MesoPumps in the planning stage, vs. ~5 achieved with present models. The ion-drag type pump, if proven feasible, might increase such efficiencies into the 60-80% range, as will be detailed below, while also decreasing the size.

Ion-Drag Pump: The proposed ion-drift pump is intended to work on the principle of viscous drag of the ions attracted by an applied e-field, so that their cumulative surface drags the neutral molecules along to the extent of establishing a force balance between this ionic drag and the drag between the induced flow and the capillary tube (or MEMS channel) wall. The former is given by the a) mobility, number density

Table 1. Comparison of Design and Performance Features of MGA Pump Technologies

Method	Base Unit Size x N		Frequency	# of Units	Power	Effic'y	Voltage
-	mm3		Hz	-	mW	%	V
Theoretical $\int V \cdot dp$	-			1	1.26	100	
Ion Drag	10 x 0.25 x 1	= 2.5	DC	1	1.65	76	40
MesoPump (E-Static, now)	10x10x1x50	= 5000	3	50	25	5	150
MesoPump (E-Static, impr.)	5x5x0.5x15	= 188	25	15	16	7.9	100
Piezoelectric Pump[7]	7x7x1.1x7x14	= 5282	100	98			

and volume of the ions in the applied e-field until they reach terminal velocity, v, as described by Stokes' Law,which relates particle radius, r, fluid viscosity, η, and the above to viscous shear force, $F_{ion}v$:

$$F_{ion} = 6\pi\,\eta\,v\,r\,N_{ions}, \qquad (1)$$

(see also list of used symbols below), and b) viscous flow "drag" of capillary flow, as described by Poiseuille's Law, which describes volumetric flow in similar terms:to $V_F = \pi r_c^2\, v = \pi\,\Delta p\, r_c^4 / (8\, L_{cs}\, \eta)$, from which we can derive the corresponding force, $F_c = \Delta P \cdot \pi r_c^2$, and

$$F_c = 8\pi\,\eta\,v_c\,L_{cs}, \qquad (2)$$

If this particle is charged, it also experiences an electrostatic force, $F_e = E\,q$, and an associated terminal or drift velocity. For a particle of charge, q, molecular mass m(N2) = 28 g/mole/N_A, experiencing an average time between collisions, τ, and subjected to the force of an electric field, E, the drift velocity is:

$$v_d = q\,E\,\tau / m = 1.6022\cdot10^{-19}(100\ \text{"V/m"})10^5\ 1.34\cdot10^{-10}/(28/6.022\cdot10^{23}) = \qquad (3)$$
$$= 4.62\ \text{cm/s per V/cm},$$

or 462 cm/s if we apply 100 V to the (+) and (-) electrodes in **Fig.3**, spaced at about 1 cm. The factor of 10^5 converts Newtons to dynes.

To arrive at the above v_d we used $\tau = 6.7\cdot10^{-6}/50{,}000 = 1.34\cdot10^{-10}$ sec, based on the average velocity of N_2 molecules in air of v = 50,000 cm/s*, and where τ = time between collisions = $\lambda / v_T = \lambda / (3kT/m)^{0.5}$, m = 28/$N_A$ = mass of a N_2^+ charge carrier, v_T = thermal velocity and λ = mean free path = 6.7 x 10^{-6} cm at 1 atm, or generally, λ = 0.005/p, with p in Torr* and λ in cm at ambient conditions, $N_A = 6.022\cdot10^{23}$ = Avogadro Number of molecules per mole, the Boltzmann constant, $k = 1.3807\cdot10^{-16}$ erg/K, and the elemental charge value of q = 1.6022 10^{-19} coulombs.

* http://www.uccs.edu/~tchriste/courses/PHYS549/549lectures/gasses.html

To determine the actual flow velocity that results from balancing the ion-drag action force and the viscous force offered by the flow in a capillary of length, L_{cs}, we set $F_{ion} \equiv F_c$, and therefore obtain

$$6\pi\,\eta\,v_d\,r_{ion}\cdot N_{ion} = 8\pi\,\eta\,v_c\,L_{cs}, \qquad (4)$$

and numerically with $r_{ion} = 1.5\cdot10^{-8}$ cm, x_{ion} = 10 ppb, v_d(100 V/cm) = 461.6 cm/s, L_{ce} = 1 cm, L_{cs} = 50 cm and r_c = 0.0050 cm

$$v_c = (6\pi/8)\, v_d\cdot x_{ion}\cdot r_{ion}\cdot N_A^*\cdot r_c^2\cdot L_{ce}/L_{cs}, \qquad (5)$$
$$= (2.3562)\cdot461.7\cdot10^{-8}\cdot1.5\cdot10^{-8}\cdot2.883\cdot10^{19}\cdot0.0050^2$$
$$= 117.6\ \text{cm/s}.$$

This flow increases with $v_d = q \cdot E \cdot \tau / m$, x_{ion}, r_{ion} and L_{ce}, while it decreases as L_{cs} is lengthened. Additional parameters are shown in **Table 2**, especially those that relate to energy consumption.

Table 2 lets a reader change the yellow-marked inputs of applied voltage, V, r_{ion}, r_c, the length of capillary in which the field is applied and the total system's capillary length, $\mathbf{L_S}$, which determines Δp for a given v_c. The rows in Table 1 then correspond to variations in the **unknown and assumed unipolar(!) ion concentration**, which then determine the macroscopic viscous flow in a capillary of length L_c and in one of length L_S, which results in a much smaller v_c due to the much larger and also-listed Δp.

The Table data show that barring minor variations in the values used above, this method of generating flow should indeed work well, and with a very small concentration of ions, provided we do not run into electron-attachment or space charge effects and can maintain electric neutrality as we pull the heavy ions through the gas. However, this is precisely what ion drift spectrometry is leveraging, and is being used as a gas detector.

As we increase the intensity of the fields applied to the MDDs (microdischarge devices) for ion generation, and drawn into **Fig.3** as multiple sets of interdigitated electrodes, the rate of ion generation, their concentration, their collective drag and the resulting macroscopic flow velocity increase. However, it does not reach or exceed the drift velocity, which just adds to the top of the gas velocity.

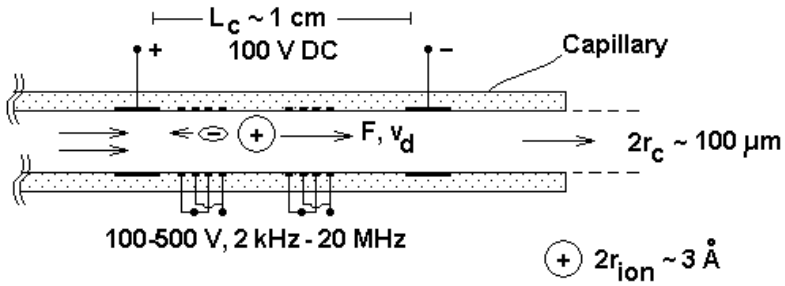

Fig. 3. Cross Sectional Sketch of Proposed Pump. High-Frequency MDDs Generate Ion-Electron Pairs. Relatively Larger Ions Drift towards (-) Electrode and Drag Neutral Molecules Along.

Table 2. Ion-Drag Pump Flow and Energy Characteristics

Applied Pot. V	Ion	Gas Velocities for Ls=Le	Ls	Re(Ls)	Δp(Ls)	Qohmic	Ion+Flow Qvisc	Qgen	Qvisc+Qgen Qtotal	Qideal	Efficiency
100	mol fraction	cm/s	cm/s	-	psid	mW	mW	mW	mW	mW	%
	3.163E-09	37.20	0.74	0.050	0.030723	0.0000531	1.238E-05	0.003465	3.53E-03	1.238E-05	3.506E-01
Ion Radius, rion cm	5.624E-09	66.15	1.32	0.089	0.054634	0.0000945	3.915E-05	0.006170	6.30E-03	3.915E-05	6.211E-01
	1.000E-08	117.63	2.35	0.159	0.097154	0.0001684	1.238E-04	0.010996	1.13E-02	1.238E-04	1.097E+00
1.50E-08	1.778E-08	209.18	4.18	0.282	0.172767	0.0003006	3.915E-04	0.019632	2.03E-02	3.915E-04	1.926E+00
	3.163E-08	371.98	7.44	0.502	0.307228	0.0005383	1.238E-03	0.035155	3.69E-02	1.238E-03	3.352E+00
Cap.Radius, rc cm	5.624E-08	661.49	13.23	0.892	0.546337	0.0009691	3.915E-03	0.063287	6.82E-02	3.915E-03	5.743E+00
	1.000E-07	1176.31	23.53	1.586	0.971540	0.0017606	1.238E-02	0.114981	1.29E-01	1.238E-02	9.588E+00
0.005	1.778E-07	2091.81	41.84	2.821	1.727670	0.0032490	3.915E-02	0.212183	2.55E-01	3.915E-02	1.538E+01
	3.163E-07	3719.83	74.40	5.017	3.072280	0.0061513	0.12380	0.401718	0.53	0.1238	23.286
Field Length, Le cm	5.624E-07	6614.89	132.30	8.921	5.463373	0.0121200	0.39150	0.791515	1.20	0.3915	32.758
	1.000E-06	11763.13	235.26	15.864	9.715403	0.0252884	1.23805	1.651501	2.91	1.2380	42.474
1	1.334E-06	15686.38	313.73	21.155	12.955698	0.0375189	2.20159	2.450234	4.69	2.2016	46.949
	1.778E-06	20918.13	418.36	28.211	17.276701	0.0567832	3.91504	3.708316	7.68	3.9150	50.976
Tot.Cap.Length, Ls cm	2.372E-06	27894.77	557.90	37.619	23.038851	0.0877265	6.96204	5.729119	12.78	6.9620	54.481
	3.163E-06	37198.28	743.97	50.166	30.722802	0.1383333	12.38045	9.034076	21.55	12.3805	57.442
50	**Drift Vel. in cm/s, vd =**	461.747									
	NA, Avogadro Num. in 1/cm3 =		2.8830E+19								
Eion, Ioniz.Energy eV	**q, Electronic Charge in Cb =**		1.6022E-19			1					
70											

MBrfc/TL-03-IonPump.xls

As the DC field is increased, changed or switched off, the macroscopic flow changes within fractions of a millisecond and can thus be used to control and/or pulse the flow in the second stage of a µGC-µGC analyzer. However, the feasibility of the proposed pump concept still needs to be proven.

The usefulness of this ion-drag pump clearly and strongly depends on:

- The density & life of the generated ions
- The differentiation in size or asymmetry between positive and negative charge carriers, and
- The asymmetric positioning and shape of the ion drift e-field electrodes.

By providing such essentials, the charge carriers will be able to drive flow of the neutral molecules, not just through its own e-field section but through and against a useful "load", i.e. against the flow restriction of a practical flow system as e.g. in a GC or μGC of column length, L_{cs}. For practical and variable inputs such as100 V/cm DC field, ion size (assumed enhanced by the attachment of polar molecules like water and a range of ion mole fractions, x_{ion}, (all inputs are highlighted in yellow), **Table 2** lists the achievable flow velocities without load (L_{cs}=L_{ce}); and for a useful load the flow velocities, v_c, the Reynolds Numbers, Re, viscous pressure drops, Δp_e, and the dissipated powers and total power and efficiencies, using as reference the ideal or theoretical power to move the gas against the listed pressure head.

An additional important consideration is the amount of power needed to not only draw and collect the ions, but to also generate and regenerate them as they drift and recombine along the e-field. We assumed in Table 2 that one would need to regenerate ions 99 times within the moving gas volume in the e-field. This may be partly redundant with the fact that the practical energy for generation of ions exceeds the theoretical ionization energy by a factor of 4-6, so that the textbook ~10-12 eV (see Table 3, using eV x 96600 Cb/mole for conversion to joules) becomes 60-70 eV in practice. The energy dissipations of the ion pump are thus composed of these elements:

1. Ionic drift viscous friction loss in the gas, which drives all, $Q_{iondrag} = F_V \cdot v_{ion} = 6\pi\eta v_{ion}^2 \cdot r_{ion} N_{ion} \cdot$
2. Gas flow viscous friction loss, $Q_{gas} = F_c \cdot v_c = 8\pi \cdot \eta \cdot v_c^2 \cdot L_{cs}$
3. Electric, ohmic power dissipation, $Q_{ohmic} = U \cdot I = U \cdot q \cdot N_{ion} \cdot (v_{ion} + v_{gas})$
4. Ion generation and (99%) regeneration, $Q_{gen} = (1+99)\, E_{ion} \cdot N_{ion} \cdot (v_{ion} + v_{gas})$
5. Work on moving (assumed incompressible) gas through the Δp, $Q_{ideal} = \int V_F(p)dp \sim \pi \cdot r_c^2 \cdot v_{gas}\, \Delta p$

Table 2 shows encouraging data, indicating that even if we need to regenerate the ion-electron pairs 99 more times due to recombination, in order to maintain an exemplary ion concentration of $x_{ion}=10^{-6}$, the ion pump would achieve ~50% efficiency!! This is for reference conditions of E = 100 V/cm, L_{cs} = 50 cm, r_{ion} = 1.5 Å, and r_c = 50 μm. The table data reveal that:

- As ion concentration increaes, so do pumping velocity, Re, Δp, all individual Qs, but also efficiency
- The power dissipated via the ionic current and applied DC voltage, Q_{ohmic}, is, surprisingly, ~100x lower than Q_{visc}, but did not have to be used in the computation of Q_{total}, which we based on the sum of the viscous dissipation of ions and capillary flow + ion generation and regeneration energy

Changing input parameters reveals further features of the pump and its present model:

- Increasing the effective ion radius by a factor of 2 increases efficiency at x_{ion}=1 ppm from 42.5 to 68.8%
- The needed generation power is only 1.65 mW for E_{ion} = 70 eV and 99% regeneration rate
- Reducing the e-field by 2x decreases flow by 2x and efficiency from 42 to 27%
- Reducing the capillary length by 2x doubles the flow velocity, maintains the pressure drop constant(!) and increases efficiency to 52.5%.

Future Work: As mentioned above, the feasibility of a practical ion-drag pump depends on the ability to configure and operate MDDs to generate the needed ion concentrations and asymmetries. By configuring MDDs in series and parallel, the desired flow and pump pressure head may be achieved. The feasibility of also achieving advantageous energy efficiencies obtained by the present model depends of the actual number and amount of power the MDDs need to move the sample gas. Descriptions of macroscopic ion-drag pump systems, such as used in Honeywell's Electrostatic Air Cleaner, show reduced efficiency as dimensions are reduced, but may be strongly dependent on the involved type of ion generation.

One type of MDDs that may be well suited for operation of micro-scale pumps may be those stabilized in arrays of orifices, as used for UV light generation[11], and sketched out in **Fig. 4**, with TBD orifice size and shape, electrode film thickness, edge smoothness and pattern; .

Other asymmetric schemes to move fluids, mention above in the Introduction, should be explored as synergistic complements to the ion pump described above.

Nomenclature: Below we list the most common physical parameters used above:

E Electric field, E = U/s, in volts / cm
E_{ion} Energy of formation of ions
F Force of electrostatic field, F_e, of ionic viscous drag, F_{ion}, or of viscous capillary flow , F_c
L_c Length of the capillary, in the applied e-field, L_{ce}, and of the whole system, L_{cs}, in cm
λ Mean free path between collisions, in cm
N Number of ions in the length of capillary between electrodes, $N = x_{ion} \cdot N_A^* \cdot \pi \cdot r_c^2 \cdot L_{ce}$
N_A Avogadro number in mol^{-1}
N_A^* Avogadro number in cm^{-3}
r Radius of capillary, r_c, or ion, r_{ion}
T Temperature in K
τ Time between collisions $\tau = \lambda / v_T = \lambda / (3kT/m)^{0.5}$, in s
x Molar or volumetric fraction of ions, x_{ion}, or molecules, x
v Velocity. 1. Ion drift relative to fluid, v_{ion}; 2. Macroscopic capillary flow, v_c, in cm/s
v_{ion} Velocity of ion drift relative to fluid. Total ion velocity = $v_{ion}+v_c$, but friction loss ~ v_{ion}.
V Volume in cm^3
V_F Volumetric flow in cm3/s
V_M Volume of one mol of gas, V_{Mo} under 1 atm and 0°C conditions

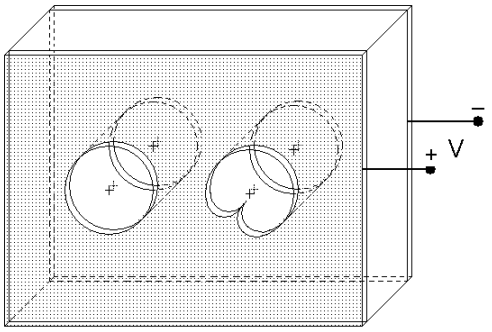

Fig. 4. Two Elements of an Array of MDDs for Ion-Drag Pumping through the Orifices. Symmetry Variation via Electrode Shape or Thickness.

References

1. R.Shannon et al, Electric Wind Generator," U.S.Pat.No. 4,210,847, assigned to the U.S.Navy, 1 July 1980
2. D.M. Sherman et al, "Paraelectric Gas Flow Accelerator, " U.S.Pat. 6,200,539, assigned to the Univ. of Tennessee Research Co., 13 March 2001
3. Cyrus Herring (Caviton Inc, Urbana-Champaign, IL), "Microdischarge-Based Detection Systems", DARPA Workshop on Micro Gas Analyzers, Monterey, CA, 16-17 Dec. 2002, CD Proceedings
4. S.-J.Park, J.G.Eden and J.J.Ewing, (Department of Electrical and Computer Engineering, Laboratory for Optical Physics and Engineering, University of Illinois, Urbana, Illinois 61801), "Photodetection in

the visible, ultraviolet, and near-infrared with silicon microdischarge devices," Appl. Phys.Lett., 81#24, 4529, 9 Dec. (2002)
5. C.J. Morris, and F. K. Forster (U.Washington, Seattle) "Optimization of a Circular Piezoelectric Bimorph for a Micropump Driver." J. Micromech. Microeng., 10 (3), 459-465. (2000).
6. C.J.Morris and F. K. Forster (U.Washington), "Low-order modeling of resonance for fixed-valve micropumps based on first principles." J. Microelectromech. Syst., 12 (3), 325--334 (2003).
7. Ari Glezer (Geogia Tech), Microjet Dev'ts, http://www.me.gatech.edu/me/people/academic.faculty/Ari.Glezer.html
8. Ted Zeller (U.Michigan), "WIMS Micro Gas Chromatograph Development," DARPA Workshop on Micro Gas Analyzers, Monterey, CA, 16-17 Dec. 2002, CD Proceedings
9. Simone Brand, Fraunhofer Institute, "Piezoelectrically Actuated Micro-Diaphragm Pump," December 1999, www.ims.fhg.de, brand@imsm.fhg.de. This 7 x 7 x 1 mm pump-chip is reported
10. Cleopatra Cabuz, William R. Herb, Eugen I. Cabuz, Son Thai Lu, "The Dual Diaphragm Pump," 14th International Conference on MEMS, Switzerland, 21-25 January 2001, p. 519-522.
11. Gary Eden (U.Illinois), Private Communications, June 2003

Appendix

Table 3. Electron Affinities and Electron Configurations for the First 10 Elements in the Periodic Table***

Element	*Electron Affinity (kJ/mol)*	*Electron Configuration*
H	72.8	$1s^1$
He	<0	$1s^2$
Li	59.8	[He] $2s^1$
Be	<0	[He] $2s^2$
B	27	[He] $2s^2$ $2p^1$
C	122.3	[He] $2s^2$ $2p^2$
N	<0	[He] $2s^2$ $2p^3$
O	141.1	[He] $2s^2$ $2p^4$
F	328.0	[He] $2s^2$ $2p^5$
Ne	<0	[He] $2s^2$ $2p^6$

Element	*Ionization Energies (kJ/mole)*
H	1300
O	1300
He	2400
C	1050

*** http://chemed.chem.purdue.edu/genchem/topicreview/bp/ch7/ie_ea.html

Table 4. Temperature Dependence of Ion Concentration

Temper. T in K	**Ion Aff. Energy E(-) in J/mol 100,000** exp(-E/RT)	**Ionizat.Energy* E(+) in J/mol 1,000,000** exp(-E/RT)
600	2.239E-09	3.169E-87
1500	3.468E-04	2.514E-35
2000	2.541E-03	1.123E-26
2500	8.395E-03	1.739E-21

by U.Bonne, 16 Oct.2003

E. Miscellaneous Information

1. JSLSCAD (Joint Service Lightweight Standoff Chemical Agent Detector)[1].

The JSLSCAD is a passive infrared (IR) detection system that detects the presence or absence of chemical warfare agents in the 800 to 1200 cm^{-1} (12 - 8 μm) IR region of the electromagnetic spectrum by monitoring the ambient background IR radiation. The JSLSCAD signal processing hardware discriminates between the chemical targets and the other nontoxic species in a complex battlefield environment.

The unit is capable of on-the-move, real-time detection from either aerial or surface platforms. The unit will detect and alarm to a chemical agent cloud up to 5 kilometers away. The detector also provides chemical identification information and data for activation of countermeasures to avoid contamination. The JSLSCAD is equipped for visual and audible alarm and can display the agent class and relative position. This information is available locally and transmission to battlefield information networks. JSLSCAD also has the capability to indicate an all-clear condition.

The problem of detecting chemical vapors in the atmosphere has been of interest to the military for several decades. It is well known that chemical warfare (CW) agents such as Mustard (H-agents), Lewisite, VX and the nerve gases (G-agents) have strong absorption features in the long-wave infrared (8-12 μm) region of the spectrum. Standoff detectors address the requirement to detect vapor clouds produced by agent releases. Methods of delivery include shells, bombs, bomblets, missiles and sprayers, generating clouds as large as 100 meters wide. Given sufficient thermal contrast between the vapor cloud and the background, it is possible to detect and identify a CW agent by remote sensing spectrometry

References

(1) JSLSCAD (Joint Services Lightweight Standoff Chemical Agent Detector), a small, fully-automatic, standoff chemical agent detector http://www.globalsecurity.org/military/systems/ground/jslscad.htm

Acronyms

- CAD — Computer Aided Design
- CPAC — Center for Process Analytical Chemistry
- CWA — Chemical Warfare Agents
- ERC — Explosive-Related Compounds
- ES&C — Embedded Sensing and Control (Honeywell Business Unit)
- DTRA — Defense Threat Reduction Agency
- GC — Gas Chromatograph or "boiling point spectrometer"
- GCD — Gas Chromatography Detectors
  - AED — Atomic Emission Detector
  - CID — Chemical Impedance Detector (Chemi-resistor or -capacitor)
  - ECD — Electron Capture Detector
  - FID — Flame Ionization Detector
  - FPD — Flame Photometric Detector, for P- and S-containing compounds
  - FD — Fluorescent Detector
  - MDD — Micro Discharge Device
  - MDID — Micro Discharge Impedance Detector
  - MDOD — Micro Discharge Optical Detector
  - NPD — Nitrogen Phosphorous Detector
  - PDED — Pulsed Discharge Emission Detector
  - PID — Photo-ionization Detector
  - TCD — Thermal Conductivity Detector
  - TID — Thermionic Ionization Detector
- IDHL — Immediate Danger to Health and Life
- IMS — Ion Mobility Spectrometer
- IVP — Integrated Vacuum Package (at the wafer level)
- NAFA — National Air Filter Association
- MDL — Minimum Detection Level
- MEMS — Micro-Electro-Mechanical Systems
- MGA — Micro Gas Analyzer
- MGC — or μGC: Micro Gas Chromatograph(y)
- MS — Mass spectrometer
- PHASED — Phased Heater Array Structure for Enhanced Detection
- PI — Principal Investigator
- PLOT — Porous-Layer Open-Tube column
- PS&C — Precision Sensors and Components (Honeywell Business Unit)
- ROC — Receiver Operating Characteristic or plot of TPF vs. FPF
  - TPF — True Positive Fraction
  - FNF — False Negative Fraction, with TPF + FNF = 1
  - TNF — True Negative Fraction
  - FPF — False Positive Fraction, with TNF + FPF = 1
- SAW — Surface-Acoustic Wave
- SSEC — Solid-State Electronics Center (Honeywell Business Unit)
- TC — Thermal Conductivity
- TFR — Thin Film Resonator
- UAVs — Unmanned Air Vehicles
- UGS — Unattended Ground Sensors

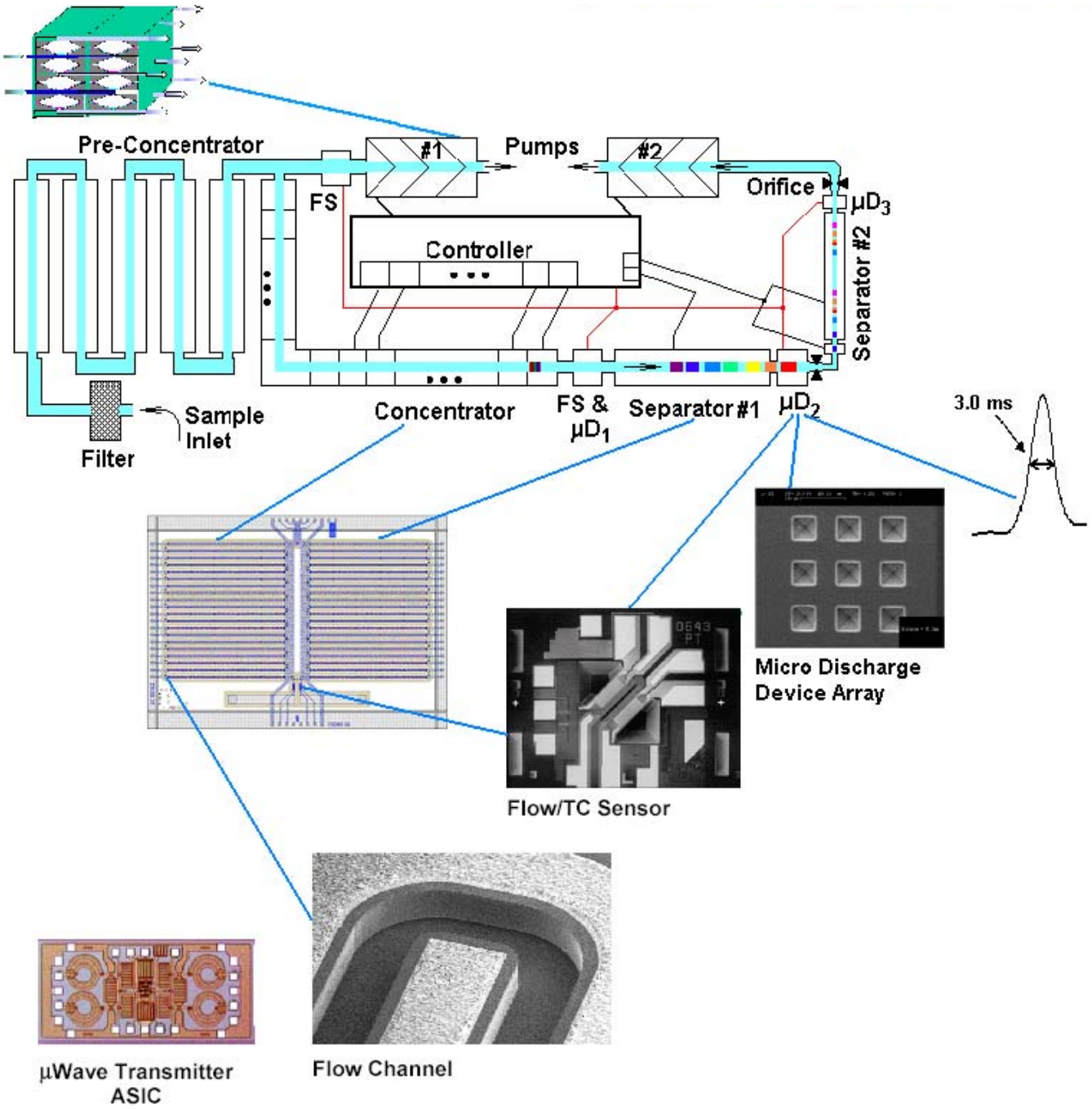
Pre-Concentrator
#1
Pumps
#2
Orifice
μD_3
FS
Controller
Separator #2
Sample Inlet
Filter
Concentrator
FS & μD_1
Separator #1
μD_2
3.0 ms
Micro Discharge Device Array
Flow/TC Sensor
µWave Transmitter ASIC
Flow Channel